Universitetet
i Stavanger

DET TEKNISK-NATURVITENSKAPELIGE FAKULTET

MASTEROPPGAVE

Studieprogram/spesialisering: Petroleumsteknologi, Reservoarteknikk	Vårsemesteret, 2014 Åpen / ~~Konfidensiell~~
Forfatter: Marcus Risanger	..... (signatur, forfatter)
Fagansvarlig: Skule Strand Veileder(e): Skule Strand & Tina Puntervold	
Tittel på masteroppgaven: Smart Water EOR in Sandstone Reservoirs	
Studiepoeng: 30	
Emneord: Smart Water Water injection Low Salinity Enhanced Oil Recovery (EOR) Wettability Alteration Clay Sandstone Anhydrite	Sidetall: 8 + 69 Stavanger, 13. juni 2014

Master Thesis
MPEMAS

Smart Water EOR in Sandstone Reservoirs

Universitetet
i Stavanger

Marcus Risanger

University of Stavanger

June 13, 2014

Abstract

This study attempts to assess the viability of injecting medium-salinity brines of 25.000 ppm NaCl as a substitute for 1.000 ppm low-salinity Smart Water for injection in sandstone reservoirs, as well as study the effect of calcium precipitates in the formation on low-salinity Smart Water effects.

Yme-18 is flooded with 25.000 ppm NaCl after it was flooded to a production plateau using 100.000 ppm formation water—zero additional oil is produced. The 1.000 ppm NaCl flood that followed induced an increased production of 4 %. It was finally concluded that the 25.000 ppm brine was found ineffective in this particular system of rock/crude oil, most likely because of the relative concentrations of the different cations present.

Yme-19 was flooded with approximately 200 pore volumes of 1.000 ppm NaCl brine before the experiment in an attempt to remove anhydrite ($CaSO_4$) from the core material. Yme-16 was flooded as little as possible, to compare results in an anhydrite rich and depleted core. While the attempt to clean out anhydrite from the core material failed, the concentration of sulfate in the critical low-salinity Smart Water interval was around 40 % lower.

Yme-19 and Yme-16 was flooded with formation water until plateau, then 1.000 ppm NaCl for an additional production of 2.5 %OOIP and 2 %OOIP, respectively. A discussion was carried out even though the additional recovery is most likely within experimental error, in light of very congruent results from the initial flooding of the two cores. The increased dissolution of sulfate and a higher initial pH was used as factors to explain the lower recovery from the Yme-16 core compared to Yme-19.

Indications of secondary wettability alteration towards a more oil-wet state by high-salinity reduction of capillary trapping was indicated in the Yme-19 and Yme-16 experiments. The proposed mechanisms and core response was discussed and the effect found plausible with the given data.

Suggestions for future work were derived from the experimental results and discussion.

Acknowledgement

Being given the opportunity to write a Master's thesis for the Reservoir Chemistry EOR group at the University of Stavanger truly is a privilege. This entire semester I have been surrounded by extremely talented people who show a very deep understanding of their field of expertise. Thanks goes out to Professor Tor Austad, Associate Professor Skule Strand and Postdoctoral Fellow Tina Puntervold for having me writing a thesis for their group, their invaluable discussion and input during and after the experimental stages, proof-reading and for sharing their vast amounts of knowledge to improve both my understanding of the problem at hand, and the thesis itself.

Special thanks goes to University of Stavanger PhD student Iván Dario Piñerez Torrijos. I am exceedingly grateful for all his assistance, helpfulness and guidance throughout the semester. I hope my work will prove useful in your doctoral pursuit, and wish you and your family the best of luck in the future.

Also thanks to the other PhD students; Hossein Ali Akhlaghi-Amiri, Paul Hopkins and Zahra Aghaeifar, for their valuable input and assistance during my stay in the laboratory.

Thanks to my fellow students in the EOR lab completing their M.Sc. and B.Sc. degrees, for sharing their opinions and discussing their results and mine, so that everyone can better understand both the results we have gotten in our laboratory experiments.

Lastly, thanks to Professor Gunnar Thorkildsen and Assistant Professor Helge Bøvik Larsen at the University of Stavanger—not only for giving me the opportunity to give back to the University by being a student assistant in several subjects during my time at UiS, but also for helping me develop the skills to utilize both LaTeX and *Wolfram Mathematica* proficiently, and being good company over the past years. It will be remembered fondly.

Table of Contents

1 Introduction **1**

1.1 Thesis Objectives 2

2 Theory **3**

2.1 Sandstone 3

2.1.1 Origin 3

2.1.2 Composition 4

2.1.3 Clay Properties 5

2.2 Reservoir Properties 6

2.2.1 Temperature 7

2.2.2 Porosity 8

2.2.3 Permeability 8

2.3 Hydrocarbon Recovery Mechanisms 9

2.3.1 Scales of Observation 9

2.3.2 Primary Recovery 11

2.3.3 Secondary Recovery 12

2.3.4 Tertiary Recovery 13

2.3.5 Smart Water Flooding 14

2.4 Forces of Oil Displacement 14

2.4.1 Gravitational Forces 15

2.4.2 Viscous Forces 15

2.4.3 Capillary Forces 16

2.4.4 Capillary Number 17

2.5 Wettability 19

2.5.1 Importance of Wetting Conditions 22

2.5.2 Important Wetting Parameters 23

2.6 Initial Wetting 25

2.6.1 Organic Material Clay Surface Desorption 26

2.7 Smart Water EOR 27

2.8 Wettability Alteration by Smart Water 27

2.8.1 Low Salinity Smart Water Flooding 28

2.8.2 Wettability Alteration by High-Salinity Flooding 31

2.8.3 Slug Injection vs. Continuous Injection 32

3 Methodology and Preparation **34**

3.1 Core Material 34

3.2 Crude Oil 34

3.3 Viscous Flooding . . . 35
3.3.1 Brine Control . . . 37
3.3.2 Effluent Collection . . . 37
3.3.3 Viscous Flooding Schedule . . . 37
3.4 Effluent Analysis . . . 38
3.4.1 Ion Chromatography . . . 38
3.4.2 pH-Measurements . . . 39
3.4.3 Density Measurements . . . 39
3.4.4 Chemical Simulation . . . 39
3.5 Brine Preparation . . . 40
3.5.1 Brine Composition and Data . . . 41
3.6 Core Preparation . . . 41
3.6.1 Core Cleaning . . . 42
3.6.2 Fluid Saturation . . . 44
3.6.3 Core Maturation . . . 47
3.6.4 Core Data . . . 48

4 Results **50**
4.1 Yme-18 Core Flooding Results . . . 50
4.1.1 Oil Production Test, Temperature at 60 °C . . . 50
4.1.2 Chemical Analysis . . . 51
4.2 Yme-19 Core Flooding Results . . . 52
4.2.1 Oil Production Test, Temperature at 60 °C . . . 52
4.2.2 Chemical Analysis . . . 53
4.3 Yme-16 Core Flooding Results . . . 54
4.3.1 Oil Production Test, Temperature at 60 °C . . . 54
4.3.2 Chemical Analysis . . . 55

5 Discussion **56**
5.1 Yme-18: Medium-salinity Flood Viability . . . 56
5.2 Yme-19 and Yme-16 . . . 59
5.2.1 Effect of Anhydrite on the Smart Water Effect . . . 59
5.2.2 Secondary Wettability Alteration . . . 63
5.3 Viability of Higher-Salinity Smart Water Fluids . . . 63

6 Conclusion **66**

7 Future Work **67**

List of Figures

1 Reservoir temperature versus depth below sea floor 7
2 Porosity-permeability Relationship 10
3 Scales of Observation Illustration 11
4 Illustrating how the wetting angle is defined 16
5 Relationship between the capillary number and residual oil saturation 19
6 Graphic Representation of Wettability 20
7 Statistical distribution of Silicate Reservoir Wetting Conditions 21
8 Oil Recovery vs. Wetting Conditions 22
9 Simulated Dissoluted Calcium concentration in NaCl Brines 24
10 Common active components on clay 26
11 Schematic of Smart Water Imbibition in Tertiary Flood 28
12 Proposed Mechanism for Acidic Organic Material Desorption from Clay Surface by Low-Salinity Flooding 29
13 Proposed Mechanism for Basic Organic Material Desorption from Clay Surface by Low-Salinity Flooding 30
14 Potential for increased recovery in a high-salinity flood 32
15 Schematic of the viscous flooding setup 36
16 Schematic of apparatus used for brine filtering 40
17 Schematic of apparatus used to introduce water to the core 45
18 Schematic of apparatus used to introduce oil to the core 47
19 Yme-18 Oil Production Test 50
20 Yme-18 Effluent Analysis 51
21 Yme-19 Oil Production Test 52
22 Yme-19 Ion Chromatography Chart 53
23 Yme-16 Oil Production Test 54
24 Yme-16 Ion Chromatography Chart 55
25 Initial Recovery, Yme-19 and Yme-16 Comparison 60
26 Yme-16 Second Formation Water Flood Production Curve 62

List of Tables

1 Minerals in Sediments Derived from a Granite Outcrop 4
2 Cation Exchange Capacity of Common Clays 6
3 High Salinity Recovery Tests in Low Salinity Formation Water Cores 31
4 Mineralogical Core Data 35
5 Oil Data 35
6 Core Flooding Sequences 38
7 Chemical Composition of Brines 41
8 Physical Core Data 48

1 Introduction

The process of extracting hydrocarbons from fluid reservoirs deep underground is imperative for everyday life as we know it. The population of the world is growing, and as a result, the global energy demands are on the rise. ExxonMobil reports in it's Energy Outlook 2014 that the expected increase in population toward year 2040 is 2 billion inhabitants. [1] The corresponding increase in annual primary energy demand is expected to be around 36% in this time period, or a massive 2.11×10^{20} J. It is expected that some of these demands will be met by means of both renewable energy sources and nuclear plants. However, it is apparent that the bulk of the demand, in the future as in the present, has to come from fossil fuel sources such as natural gas, oil and coal. The fossilized energy sources account for over 82 % of the global energy consumption.

Even though energy companies believe that the fraction of the energy demand met by fossil fuels is in decline with the rise in popularity of exploitation of renewable energy sources—the 2040 forecasts assume that the demand met with fossil fuels will be as high as 77 %. This means that even though the relative consumption of hydrocarbons is reduced, the production of hydrocarbons must increase to accommodate to the increased demand. Oil production must in fact increase by around 7.1×10^6 BOE/d to account for this discrepancy.

With this in mind, and also recalling that our available hydrocarbon resources are finite, it is important for our energy future that the upstream petroleum business as a whole work to make sure that every reservoir is developed in the best possible way. Since every reservoir is different, the best choices in development naturally vary, and the efforts will have to be tailored to each case. Because of the importance of water flooding in virtually any recovery scenario—gaining a deeper understanding of the mechanisms surrounding this technique is crucial, as is developing a better idea of how we can optimize these operations.

1.1 Thesis Objectives

The main objective of this thesis is to investigate whether it is possible to get Smart Water effects in sandstone reservoir cores which contain a high amount of clay—but are otherwise relatively mineralogically clean—by injecting a brine with medium-salinity, much higher than that of traditional low-salinity Smart Water brines—in this case 25.000 ppm NaCl compared to 1.000 ppm. The viability of such medium-salinity brines will be discussed.

A secondary thesis objective is to compare reservoir cores containing different amounts of sulfate precipitates, mostly in the form of anhydrite, and its impact on the low-salinity Smart Water effect. To this end, identical flooding schedules will be used on two cores with different anhydrite content.

An attempt to induce a secondary wettability alteration will be carried out and discussed. This will be attempted by re-injecting high-salinity brine after a low-salinity flood, where the goal is to reduce the capillary trapping of oil globules in the formation left after the increase of water-wetness induced by the low-salinity flood.

2 Theory

2.1 Sandstone

2.1.1 Origin

Sedimentary rocks are formed from the burial, compaction and diagenesis of accumulated mineral and detrital particles. Organic, or detrital, material originate from living or decomposed organisms whereas mineral based, clastic, sediments generally originate from physical and chemical weathering of tectonically uplifted rocks. The weathered rocks can be of igneous, metamorphic or sedimentary origin. [2] Mineral particles undergo further weathering during the transportation from erosional surface to depositional basin, where they break into successively smaller rock shards. Sediment which have been transported further from source to sink often consist of harder mineral types, as softer minerals are weathered more quickly into clay particles over the course of transportation. An example of mineralogical composition with regards to weathering is shown in Table 1.

Deposition initiates as soon as the flowing velocity of the transport medium goes below a grain size dependent threshold. [2] Below this threshold, the flow will no longer be able to transport the grains. The grains start to accumulate. For some depositional environments, this can happen when a river or stream flows into a larger body of water, whence the flow velocity quickly drops, in accordance to the famous Bernoulli equation. [3] Sediments can also be transported by wind, as is the case for e.g. aeolian dunes—the flowing medium does not have to be liquid. If the sediment aggregates in a sedimentary basin, it can be superposed by several additional sedimentary layers in a successive fashion and eventually be completely buried and compacted, before finally it will lithify under high pressure and temperature.

Table 1: Minerals Present in Sediments Derived from a Granite Outcrop Under Varying Intensities of Weathering. [4]

Intensity of Weathering		
Low	Medium	High
Quartz	Quartz	Quartz
Feldspar	Feldspar	Clay Minerals
Mica	Mica	
Pyroxene	Clay Minerals	
Amphibole		

2.1.2 Composition

Sand, which lithifies into sandstone under high pressure, is generally defined as siliciclastic sediment consisting of medium-sized rock particles ranging from 62 μm to 2 mm in diameter, which means that the grains are visible to the naked eye. [5] Composition of the mineral grains vary to some degree, but is usually mainly quartz (SiO_2) with small amounts of feldspar, mica, biogenic particles, and traces of many other mineral types.

During the diagenetic process, grains are coated in a form of cement made up from precipitation of previously chemically dissolved minerals. [6] Cements are commonly made up of silica, calcium carbonate, iron oxides and clay minerals. Different coatings of the grains can have different effects on the reservoir properties.

Specifics of organic matter will not be discussed, as it is of more importance with regards to discussions concerning source rock formation, kerogen types and maturation, topics which are not covered in this thesis.

2.1.3 Clay Properties

All reservoirs will have some fraction of clay present in the bulk rock volume. The clay content degrades the reservoir quality because it increases the residual water saturation and can severely alter the permeability of reservoir zones, and ultimately also completely block pore throats.

It is crucial to understand the behavior of the clay present in the reservoir because of two special properties;

- Cationic Exchange Capacity (CEC)
- Swelling

Firstly, parts of the clay surface are negatively charged; in part because of variations of ions in the clay structure, partly because of broken bonds at the edges and surface, and lastly because of dissociation of accessible hydroxyl groups. [7] These negatively charged sites attract cations to the clay surface, where weak bonds can be established. Cations can readily be exchanged for other cations as a result of this low bonding strength. Because of their ability to exchange cations adsorbed to the external surfaces and between the layers of the clay structure, clay minerals are often referred to as cation exchange materials. [8]

The relative affinity to the clay surface of cations is referred to as the *replacing power* of the different cations in solution, which in room temperature is believed to be the following;[9]

$$Li^+ < Na^+ < K^+ < Mg^{2+} < Ca^{2+} < Sr^{2+} < Ba^{2+} \ll H^+$$

The replacing power also depends on relative concentrations of the different cations. A cation with lower replacing power can still replace ions with higher affinity if the relative concentration is high enough. Hydrogen is active toward the clay surface down to very low concentrations. By controlling these

concentrations, it is possible to control, to some extent, which cations adsorb onto the clay in the reservoir rock.

Different clays have different cationic exchange capacity, refer to Table 2 for comparison of common types of clay found in sandstone reservoirs.

Table 2: Cation Exchange Capacity of Common Clays in Sandstone Reservoirs. [9, 10]

Clay Type	CEC [meq/100g]
Kaolinite	3–15
Illite	10–40
Chlorite	10–40
Montmorillonite	70–150

Lastly, while not imperative for the scope of this thesis, it is also important to keep in mind that some clays are prone to swelling. Different clay configurations behave differently and display various degrees of swelling depending also on the injection brine. It is very clear, however, that any swelling behavior will not contribute positively to the reservoir quality, and should be avoided. [11]

2.2 Reservoir Properties

Siliciclastic reservoirs account for around 74 % of the world's hydrocarbon reservoirs, and in turn account for around 60 % of the world's hydrocarbon daily production. [2, 12] Consequently, understanding the reservoir properties associated with this type of reservoir rock is instrumental in improving global recovery factors.

The most important of these properties with regards to microscopic recovery mechanisms will be discussed below.

2.2.1 Temperature

Reservoir temperatures are dependent on the depth in the Earth crust and the regional temperature gradient. Most reservoirs will therefore lie within a temperature range of 14 to 36 °C/km. Ehrenberg *et al.* [13] prepared an extensive analysis of the distribution of temperatures in the Gulf of Mexico, shown graphically in Figure 1.

This data is important because some parameters e.g. phase miscibility [14] depend heavily on temperature. Chemical reaction speed can also vary with reservoir temperature, depending on the type of reaction (exo- vs. endothermic).

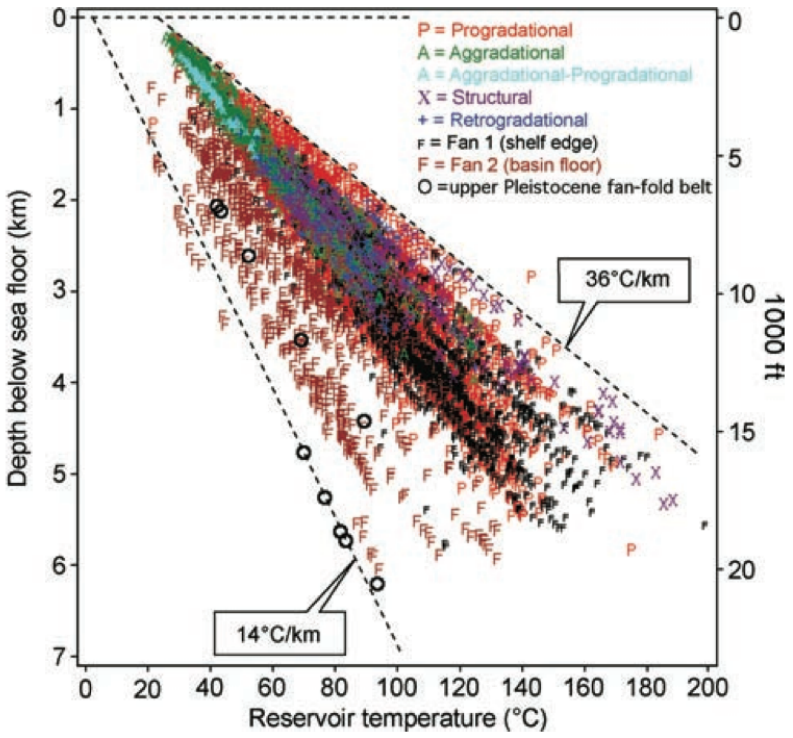

Figure 1: Reservoir temperature versus depth below sea floor. Plotting symbols indicate play type. [13]

Deep reservoirs located in a region with a particularly steep temperature gradient can exhibit very high reservoir temperatures which in turn may hinder some types of recovery processes because of sub-optimal conditions. In addition

to impacting the feasibility of different forms of EOR, the temperature is also a dependence of wetting, which will be discussed in Section 2.5

2.2.2 Porosity

Porosity, most often denoted ϕ, is normally defined as the ratio of the volume of the pores to the total rock volume. In hydrocarbon reservoirs, different types of porosity can exist; the most important of which is the intergranular porosity, which is the void space between individual grains. There is also intragranular porosity, which is the void space within grains, fracture porosity which is the void space between fracture surfaces. Vugular porosity and cavities can also occur, most often found in reservoirs which contain minerals prone to dissolution. [15]

It is also necessary to distinguish *effective* and *total* porosity. Where the total porosity includes all void space in the rock volume, effective porosity only takes into account the *connected* void space in the rock. The effective porosity is always lower than the total porosity, and the ratio can vary with respect to grain size and sorting, the degree of post-depositional cementation and precipitation of clay formations blocking pore throats.

2.2.3 Permeability

Perhaps the least intuitive reservoir parameter is the permeability; how well the rock can transmit fluid with a given pressure differential, cross-sectional area and fluid viscosity. A simple, one dimensional version of Darcy's Law can be found in Section 3.6.4, Equation 15.

As we can understand from the definition, a higher permeability represents lower fluid flow resistance in the reservoir. Usually, permeability is a very heterogeneous parameter and can display heavy local variation, caused by e.g. clay (which can block pores), faulting, fractures, layering and secondary porosity phenomena like dissolution of matrix to form vugs and cavities.

To complicate matters, the permeability of a rock body when two or more phases are flowing is drastically different from single phase conditions. The relative permeability for each phase is dependent on both the total permeability, the saturation of each phase and their respective viscosity, as well as the capillary pressure between the phases.

Permeability and porosity are usually regarded as properties with a dependence on each other, and they also vary with depth. Increasing the depth of an arbitrary unit volume of rock also increases the overburden pressure of this volume, which increases the compaction and reduces the pore space and subsequently the permeability of the rock. Nadeau *et al.* [16] did extensive research on the porosity-permeability relationship, data which is presented in the below Figure 2.

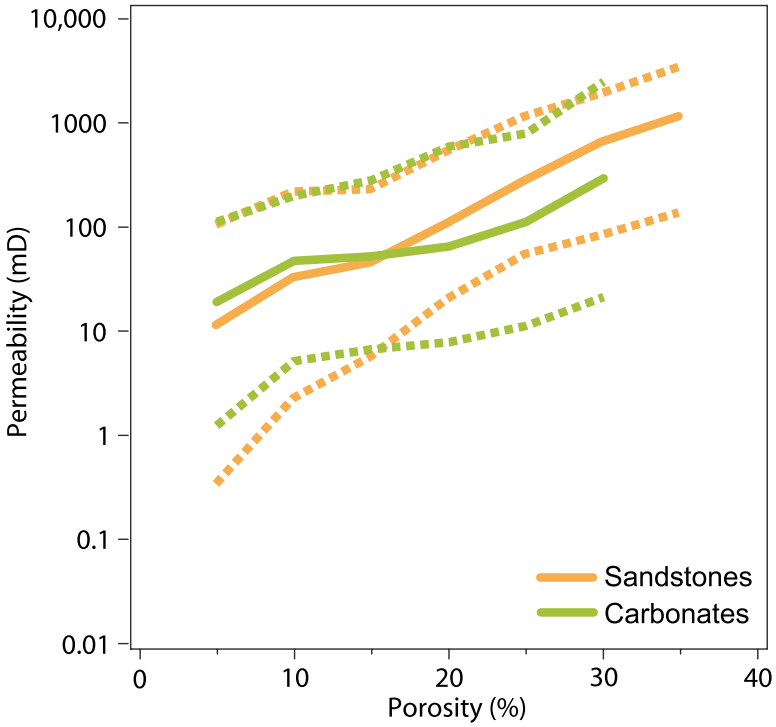

Figure 2: Statistical relationship between porosity and permeability for over 40.000 reservoirs. [16]

2.3 Hydrocarbon Recovery Mechanisms

Mechanisms of hydrocarbon recovery have traditionally been grouped into three main categories, where the division is chronological, based on when it is likely that the technique will be implemented. In modern field development, complementary secondary and tertiary recovery methods are often active at an early stage of production, and sometimes even from the start of field life. In other words, the chronological gap between secondary and tertiary recovery mechanisms is becoming less intuitive.

2.3.1 Scales of Observation

Successful field development aims to maximize the rate of production as well as the expected ultimate recovery. In this quest, it is important to understand the reservoir both at a macroscopic and a microscopic level, as shown in Figure 3, both dynamically and statically. The large scale perspective encompasses e.g. the geologic structure, compartmentalization, layering, fracturing and faulting of the reservoir. This kind of information is mostly recovered from logging drill wells and large scale collection of seismic mapping. Opposing this, we also have to understand how the oil moves on a small scale. Small in this respect can range from several meters worth of reservoir rocks down to true pore-scale. Oil recovery mechanisms are usually formed on the basis of the knowledge gathered from investigating the behavior of the microscopic displacement.

The gap between large and small scale is bridged through computational upscaling, which is a technique which gives reasonable insight into highly uncertain parameters when evaluating a full-scale model from a small set of finite data points. Only when the understanding is sufficiently complete it is possible to develop fields in the apparently most efficient manner, with the tools that are available to assist in that regard.

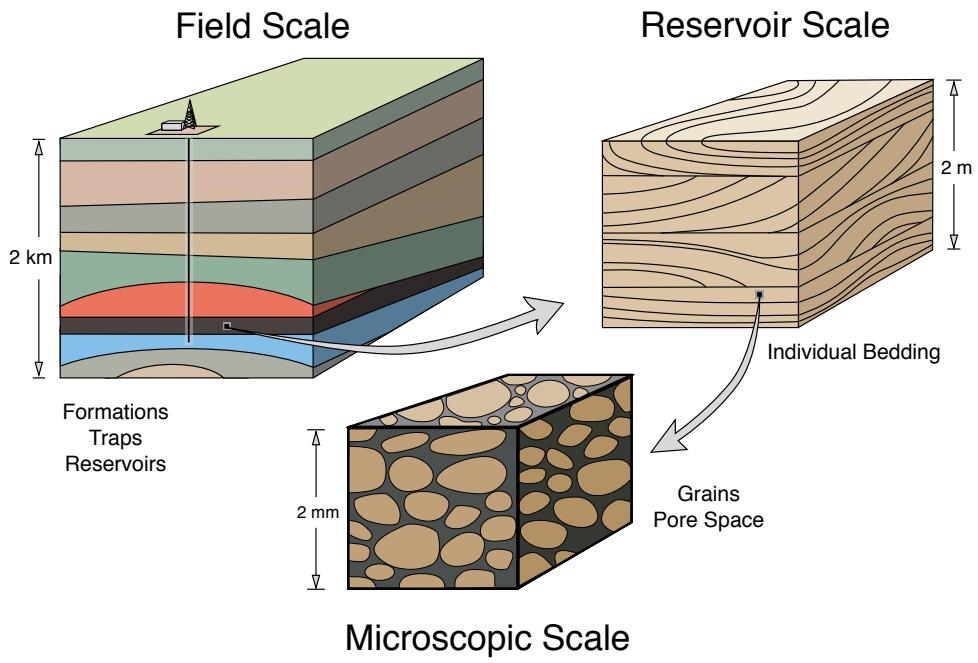

Figure 3: Illustrating the importance of scales of observation. (Adapted from SPE white paper [17])

2.3.2 Primary Recovery

The primary recovery mechanisms rely on exploiting the natural energy present in the reservoir or reservoir boundaries. [18] This simply means that the reservoir pressure is used to transport fluids out of the reservoir. There are a number of primary recovery mechanisms including the following; [19]

- Gravity Drainage
- Gas-Cap Drive
- Dissolved Gas Drive
- Aquifer Water Drive

The effectiveness of these recovery mechanisms vary greatly, but in most cases, the primary recovery range 5 % to 30 % of the Original Oil in Place (OOIP). Usually, the primary recovery stage consists of one or more of the above

mechanisms coupled together with fluid- and rock expansion which happens due to the pressure dropping in the system.

2.3.3 Secondary Recovery

As the field matures and the fluid offtake from the reservoir is increased, the natural energy drive will eventually deplete. Ultimately, the reservoir pressure will decline to a point where it is no longer sufficient to sustain production of hydrocarbons. At this point it is necessary to stimulate the reservoir to allow for production to continue. The goals of this stimulation are the following; [19]

1. Reservoir pressure is to be maintained
2. Actively displace hydrocarbons toward producing wells

The points of injection will therefore have to be chosen strategically according to reservoir models and simulations, so as to maximize the benefit of drilling additional wells. Pressure stimulation can be introduced by different methods, both continuous and discontinuous, traditionally including the following;

- Water Injection
- Gas Injection
- Water Alternating Gas Injection (WAG)

The secondary recovery phase is generally considered at an end once the production wells approach uneconomical oil rates, which for an offshore oil reservoir usually means that the water- or gas cut is very high, indicating that a large portion of the produced wellstream actually originates from the injector. Consequently, the remaining potential of the secondary recovery is very low.

2.3.4 Tertiary Recovery

Tertiary recovery techniques, or EOR methods, aim to recover additional oil compared to what is possible during primary and secondary phases of

production. When the secondary recovery phase reaches its economical limit of oil production, there is still significant volumes of oil left trapped in the reservoir as residual oil. Phase trapping is a result of the interplay between pore structure, fluid-rock interaction and fluid-fluid interactions. [19]

All EOR methods are based on injections into the reservoir, where the injection carries effects to make the reservoir conditions more favorable for the displacement of oil. These methods usually fall into one of the following categories;

- Mobility Control Processes
- Miscible Processes
- Chemical Processes
- Thermal Processes

Where the different methods have different requirements with regards to the reservoir conditions and fluid types in question. [19] Lately, there has been lots of focus on developing new EOR techniques in order to maximize discovered field potential. [17] With the current high oil prices which are forecasted to be rising [20, 21] and concern over future oil supplies, the interest in EOR processes is increasing. The available reserves can significantly increase even with small incremental gains in recovery factors.

Ultimately, EOR can be both risked based projects which require lots of planning, or simple steps taken in the early stages of reservoir development which can lead to significant value creation over time.

2.3.5 Smart Water Flooding

One EOR method which has been researched for a long time and is of high importance is Smart Water flooding. This type of EOR operation uses different kinds of brines, ranging from simple low-saline solutions to chemically optimized

brines to increase the recovery of oil from the reservoir. The benefits of Low-Salinity flooding is that it can be very cheap to implement, and given the right reservoir conditions and fluid properties, it can be highly effective.

To give an example of this—BP have already introduced a full-scale low-salinity Smart Water injection project at the Clair Ridge field, and are expecting over *40 million barrels* of increased recovery, at a cost of only 3 $/additional barrel. [22] Research is trying to establish when and, why the recovery is increased, both in sandstone and carbonate reservoirs, and how we can predict whether a field will benefit from this type of EOR mechanic.

Another benefit of Smart Water flooding is that as it is simply a chemical EOR method, which makes it able to be used in conjunction with e.g. mobility control processes. The different styles of EOR injections can therefore have a symbiotic effect where the benefit can be greatly increased.

Smart Water injections will be discussed in more detail in Section 2.8.

2.4 Forces of Oil Displacement

In a reservoir setting, there are three types of forces that are capable of driving the movement of fluids through the pore network;

- Gravitational Forces
- Viscous Forces
- Capillary Forces

These different forces will be briefly outlined in the following sections.

2.4.1 Gravitational Forces

Gravitational forces apply to two- or multi-phase reservoirs and act to segregate phases based on phase density. The gravitational forces are most important when the phases in question have large differences in density, if the IFT between the

phases is very low, or the reservoir formation is thick. [23] What can happen in these cases is called gravity override (or underride, depending on the relative density of the fluids), which means that the displacing phase goes over (or under) the phase intended to be displaced, which lowers the sweep efficiency of the operation. The buoyancy force is given below in Equation 1;

$$\Delta P_g = \Delta\rho\, g\, H \tag{1}$$

Where ΔP_g is the differential pressure due to gravity, $\Delta\rho$ is the density difference between the phases, g is the acceleration of gravity and H is the height of the hydrostatic column.

In experiments with core samples, the gravitational effects are negligible, as the potential difference in less than 4 cm of porous medium is very small.

2.4.2 Viscous Forces

Viscous forces arise from lateral pressure differentials forcing the reservoir fluid to move through the pore network of the reservoir rock body. These forces must be larger than the capillary forces in order for the fluid to flow. If the porous network is seen as a number of capillary tubes, the pressure drop across each capillary can be calculated by the Hagen-Poiseuille equation, seen below as Equation 2, which is derived from the Navier-Stokes equations.

$$\Delta P = \frac{8\mu L\bar{u}}{r^2} \tag{2}$$

Where ΔP is the pressure differential across the capillary tube, μ is the viscosity of the flowing fluid, L is the length of the capillary tube, $\bar{u}$ is the average flowing velocity of the fluid and r is the capillary tube radius.

2.4.3 Capillary Forces

The capillary forces arise from the interplay of surface- and interfacial tensions between fluids and rock, pore size and geometry and the wetting characteristics of the rock-fluid system. Capillary pressure surface forces can both hinder and aid the displacement of one fluid by another, depending on the direction of the force relative to the direction of fluid motion. [24] Equation 3 shows a simplified version of the capillary pressure;

$$P_c = \frac{2\sigma \cos\theta}{r} \tag{3}$$

Where P_c is the capillary pressure, σ is the interfacial tension (IFT) between the two immiscible phases, θ is the contact- or wetting angle and r is the capillary radius.

There is no single accepted way of measuring the contact angle or system wettability. [25] However, for a two-phase system, the contact angle can be defined by measuring the angle between the pore wall surface and the denser of the two phases, shown graphically in Figure 2.5. The measurement itself can be carried out in a number of ways, but how this can be done will not be discussed.

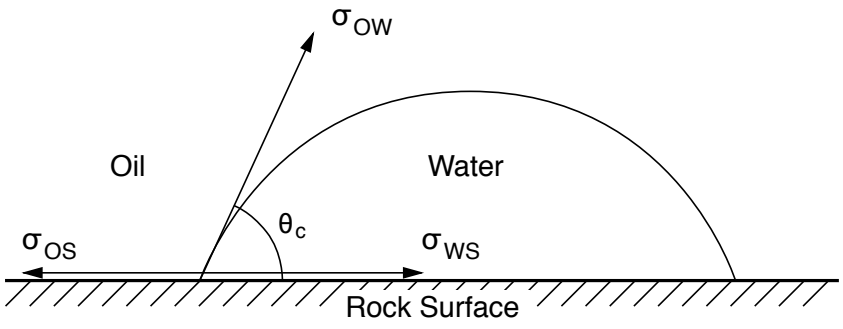

Figure 4: Illustrating how the wetting angle is defined [26]

For fractured reservoirs, strong capillary forces are desired because increased capillary pressure leads to more spontaneous imbibition of water away from the

fracture channels into the matrix blocks, increasing the displacement of oil from the lower permeability zones. Sandstone reservoirs are usually not very fractured, as opposed to carbonate reservoirs, which favors the mechanics of low capillary pressure causing less residual oil entrapment. The capillary pressure can be lowered by modifying the oil-water IFT and/or changing the contact angle.

2.4.4 Capillary Number

The capillary number, denoted N_c, relates the different displacement forces into a dimensionless property, and is really a ratio of two existing dimensionless numbers used in fluid dynamics; the Froude (Fr) and Weber (Wb) numbers. The capillary number is the ratio of viscous forces to surface tension, as seen in Equation 4.

$$N_c = \frac{\mu v}{\sigma} \tag{4}$$

Where v is interstitial velocity, μ is the viscosity of the displacing phase and σ is the surface tension. To explain the final form of the equation, given in Equation 5, we factor in that the interfacial tension is acting across a two-phase immiscible fluid interface.

$$N_c = \frac{\mu_w v}{\sigma_{ow} \cos\theta} \tag{5}$$

The capillary pressure will therefore depend on the interfacial tension between these two phases, σ_{ow}, as well as the wetting angle θ—as was discussed in Section 2.4.3. The benefit of using the capillary number as a metric arises when studies indicate that there is a relation between this dimensionless property and residual oil saturation in reservoirs. Moore and Slobod [27] suggested that the relationship improved if the viscosity ratio of the displacing and displaced phase was taken into account, as shown in Equation 6.

$$N_c^\star = \frac{\mu_w \nu}{\sigma_{ow} \cos\theta} \left(\frac{\mu_w}{\mu_o}\right)^{0.4} \tag{6}$$

Where the subscripts w and o denote displacing and displaced phase, respectively. Abrams compared the regular and modified capillary number in a large study of several reservoir cores. His findings are shown graphically in Figure 5. Qualitatively, the data shows the importance of maximizing the ratio between viscous forces and capillary forces, whence the capillary number approaches 1. Drawing from Equation 6, we see that this ratio can be altered by adjusting key variables in a beneficial way;

- Increasing flow velocity
- Creating favorable mobility ratios
- Lowering the interfacial tension
- Optimizing the contact angle

It is immediately clear that we cannot change the flow velocity because of the large pore volumes associated with a reservoir, and injectivity problems because of the large volume of injection water needed for this type of flow augmentation.

Favorable mobility ratios can be achieved with high viscosity polymer injections, which can help control the injection—but polymer injections are expensive and even great planning does not ensure a successful polymer operation, if the polymer retention in the formation is much greater than anticipated through experimental work.

Lowering the IFT can be achieved by adding surfactants to the injection water, but this type of operation can struggle with the same issues as the polymer operations; expensive and field wide applications cannot be tested beforehand.

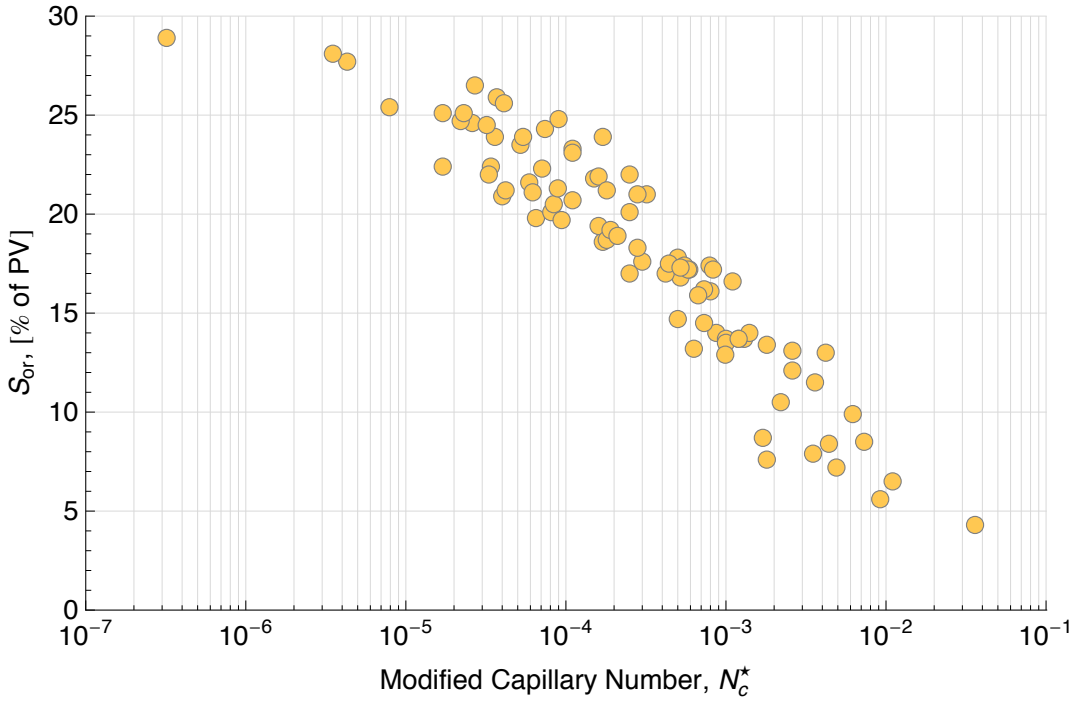

Figure 5: Illustrating the relationship between $N_c^\star$, the modified capillary number given in Equation 6 and the residual oil saturation, S_{or}. (Redrawn with data from Abrams' paper [28])

This leaves optimization of the contact angle, which basically means that the state of wettability in the formation has to be changed. We see from Equation 6 that the capillary number is maximized when the angle approaches 90°, as the cosine term in the denominator will approach 0. The wettability in the reservoir should be altered to be more neutral wet—as this appears to increase the potential oil recovery.

This is macro scale theory, how it works when looking at the reservoir as a whole. Microscopic evaluation is also needed, to understand why different EOR techniques work for different types of reservoirs.

2.5 Wettability

The wetting angle, discussed in Section 2.4.3, gives us information about which immiscible phase is more readily sticking to the pore walls. Wettability can be

described as:

> "The tendency of one fluid to spread or adhere to a solid surface in the presence of other immiscible fluids." [29]

Wetting is shown conceptually in Figure 6, for both strongly water wet and strongly oil wet systems. In the water wet case, the residual water saturation is present around the individual grains, whereas the oil phase is continuous between the oil grains. In the oil wet case, the residual water saturation is present as discontinuous globules in the pore centers, surrounded by the oil phase which is also wetting the grain surfaces.

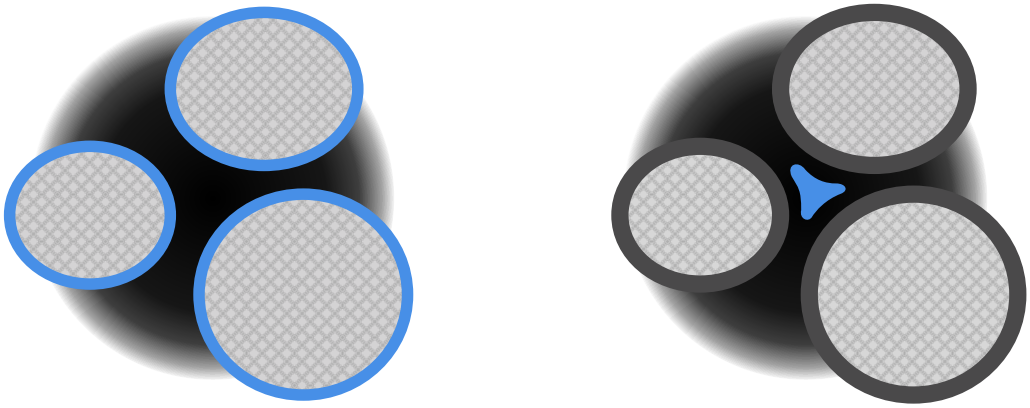

Figure 6: Graphic conceptual representation of water wet and oil wet pores.

We recall that the wetting angle is used in calculating the capillary pressure. The wetting angle is an adequate way to measure wetting conditions on discrete surfaces and simple capillaries. For porous media crude-oil/brine/rock systems, other methods are often used, i.e. the Amott method or USBM. [30, 31] It turns out, however, that the results obtained using a contact angle approach on rough surfaces can be reasonably indicative of the actual porous media wetting.

In a simplified water-oil two phase system, a neutral wet system is usually defined as having a wetting angle of 90°. Wetting angles of preferentially water wet

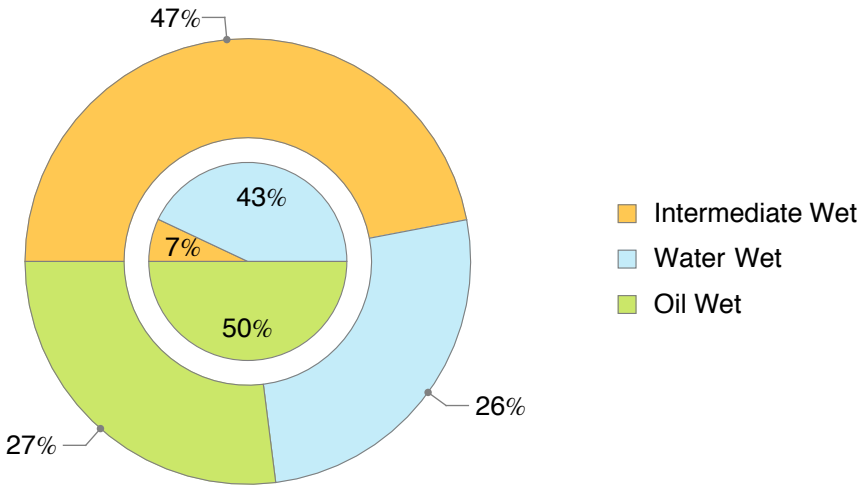

Figure 7: Statistical distribution of Reservoir Wetting Conditions in 30 Silicate Reservoirs. Data from Tarber (inner sector) [32] and Morrow (outer ring) [33], adapted for presentation.

and oil wet systems are lower and higher than 90°, respectively. This crude scale is used for the sake of simplicity; scales ranging from strong water wet, through intermediate wetness to strong oil wet are often used to better describe degrees of wetting.

A study covering 30 silicate reservoirs carried out by Tarber *et al.* [32] indicated that sandstone reservoirs are most often either oil- or water wet, with comparatively few being intermediate wet. This study has since been criticized by Morrow [33] who argued that if the contact angle interval for intermediate wetness was expanded, and hysteresis on smooth surfaces was taken into account in the Tarber study—the vast majority of the reservoirs would be either intermediate wet or water wet. The combined findings of the two papers are displayed graphically in Figure 7.

2.5.1 Importance of Wetting Conditions

The wetting conditions of the reservoir dictate not only which fluid is more readily sticking to the pore wall surface, but also affects capillary pressure and relative permeability curves for a two-phase flow. Studies show that the optimum wetting conditions with regards to recovery is that of neutral wet to slightly water wet, as shown conceptually in Figure 8. [34]

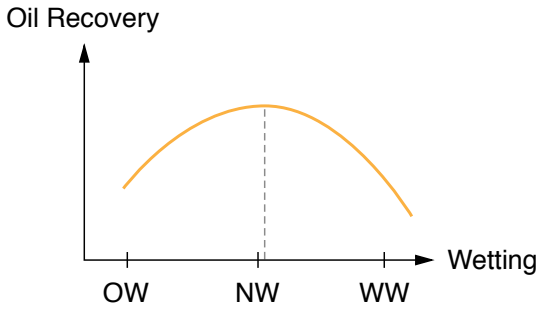

Figure 8: Maximum Oil Recovery vs. Wetting Conditions, maximum oil recovery at neutral to slightly water wet conditions. Adapted from Strand *et al.* [35]

It is clear from these findings that changing the wettability conditions towards a more neutral-wet state is likely to increase the recoverable reserves. The data also suggests that the majority of reservoirs are in a condition of wettability other than intermediate wet, and that the total potential for increased recovery is possibly quite high.

Uncovering the underlying mechanisms of wettability alteration, and how to properly utilize these mechanisms to maximize oil recovery, will enhance our understanding of field optimization for newly discovered assets. Risk associated with carrying out EOR operations can also be impacted by this, as the screening process for possible EOR methods can be made more rigid.

2.5.2 Important Wetting Parameters

The interrelation between the crude oil, formation water and reservoir rock in a crude oil reservoir makes up the basis for the wetting conditions. Additionally, temperature can affect the system with regards to reactivity of different components and the solubility of different substances. Given the number of minerals, ions and hydrocarbon components that can be present in such a system, it is impossible to describe such a system chemically, while covering all single-component equilibrium conditions.

As discussed previously, the wetting conditions are really just a relative measurement of surface affinities between the fluid phases present in the reservoir and the rock surface. How the main components in the equilibrium can affect wettability will be outlined below.

- **Reservoir Rock**

Section 2.1.2 explains the composition of a typical sandstone rock. The quartz typically makes up a very large portion of the rock and is usually negatively charged in the pH-ranges that are of interest in a reservoir setting. [36] Clay is also present in the rock, usually up to 25 wt% in developed fields, as higher clay content normally correlates to bad reservoir porosity. As discussed in Section 2.1.3, clay has permanent negative charges and is capable of cation exchange with the surrounding brine. The negative charge locations can be occupied by cations such as Ca^{2+} and H^{+}, but also organic components, all dependent on concentrations and the affinity towards these locations.

A slew of minerals can also be present in the reservoir rock. For the core samples chosen for these experiments, only calcite cementation around the grains ($CaCO_3$) and presence of anhydrite ($CaSO_4$) are of interest. Anhydrite solubility lowers as temperature increases, and can dissolve in a low-salinity flooding which increases the concentration of Ca^{2+} in the flood, which can affect

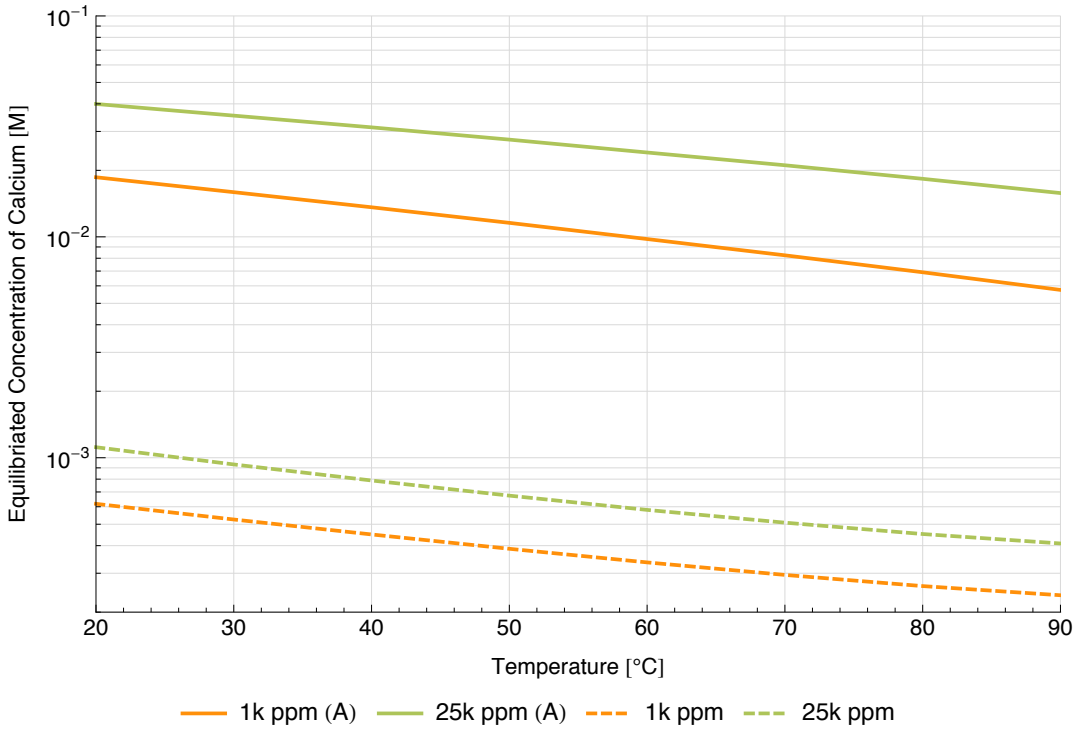

Figure 9: Dissolved Calcium concentration in 25.000 ppm and 1.000 ppm NaCl brines. Solid curves represent systems equilibriated with both calcite and anhydrite. Dashed curves represent systems equilibriated with calcite alone.

the cation exchange at the negative charge locations on the clay.

Equilibrium simulations of the calcium concentration in 25.000 ppm NaCl and 1.000 ppm NaCl brines equilibriated with calcite both in the presence and absence of anhydrite is shown in Figure 9. The simulations show that the presence of anhydrite greatly increases the calcium concentration in the brine at equilibrium, while the concentration is quite low if the system is equilibriated without anhydrite present. It is also seen that dissolution is higher in the more saline brine.

- **Formation Water**

The formation water is important both because the ionic composition dictates initial pH of the reservoir, but also because the ionic composition of the formation water is equilibriated in the reservoir system. Presence of acidic gases like CO_2 and H_2S in the reservoir fluids means that the pH is very often acidic, in the

range of 5 to 6.5. Some minerals like Albite (Plagioclase), can in turn create an alkaline environment in the reservoir given the presence of a reasonably low-saline formation water.

- **Crude Oil**

With regards to surface wetting properties, the acidic and basic material in the crude oil is the most important factors. Acidic material is mostly represented by the carboxylic group, R−COOH, whereas the basic material contains nitrogen as part of aromatic molecules R_3N, or protonated as R_3NH^+. Both acidic and basic organic material have affinity toward the clay surface, and especially in protonated form. Interestingly, the pKa of the acidic and protonated basic form is similar, at around 5. This means that the concentration of these substances in the crude oil vary similarly with regards to pH, and that the maximum adsorption onto the formation clay minerals occurs at pH $\simeq$ 5.

The polar components bonded to the clay surface act as anchoring molecules for crude oil, allowing oil to wet the surface. [35] A high content of either acidic-, basic material or both, is therefore needed to allow for making the clay surface preferential oil-wet.

- **Formation Temperature**

The reservoir temperature dictates the reactivity of the ions and the solubility of different compounds. The increased reaction speeds allow for a quicker equilibriation time. Reactivity of divalent ions increases as the temperature goes up, because of lowered hydration energy. This increases the clay surface affinity of these ions, but can also lead to precipitation of minerals such as anhydrite.

2.6 Initial Wetting

The initial wetting of a reservoir is controlled by, and depends on, the parameters discussed in the previous Section 2.5.2. Most important is the clay content, which

allows systems to become more oil wet upon initial imbibition of hydrocarbon, due to the active negative sites on the clay particles. We recall from Section 2.1.3 that Na^+, Ca^{2+} and H^+ are reactive towards these active negative surface sites, and are both ions that you can find in relatively high concentrations in the reservoir. Together with the acidic and basic organic components, these ions will compete for the active sites on the clay, where both concentration and affinity are factors which dictate the adsorption behavior of the system. This means that the five most common forms of active site clay surface bonding are therefore as shown in Figure 10.

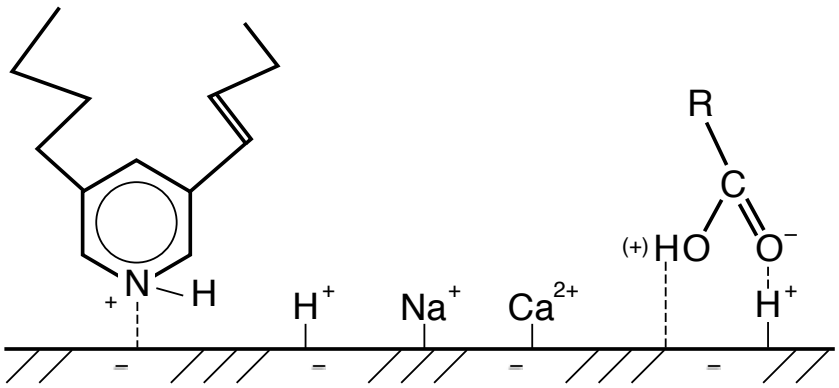

Figure 10: Most common active components toward the clay surface in the reservoir, adapted from Strand *et al.* [35]

The basic material bonds to the negative site by electrostatic interaction, whereas the acidic material is bonded using a hydrogen bond. When the organic material has bonded to the surface of the clay, they can act as anchors for the other oil particles. This means that without acidic or basic material in the crude oil, it is much less likely to encounter oil wetness.

2.6.1 Organic Material Clay Surface Desorption

In order to profit from having organic material adsorbed to the clay surface, it is necessary that this process can be reversed, in such a way that other cations

replace and subsequently release the organic material bonded to a negative site on the clay surface. Studies on adsorption and desorption of the basic material Quinoline onto Kaolinite clay was carried out by RezaeiDoust *et al.* [7], where the results show that the process is completely reversible. As for acidic material, the same trend can be seen in an experiment using Benzoic acid and Kaolinite, where the adsorption increases by over one order of magnitude when souring the brine from pH 8.1 to 5.3, which suggests that the protonated form of the acidic organic components has a higher affinity toward the clay surface. [37]

Consequently, any organic material adsorbed on clay surfaces in the reservoir can be desorbed and released, a reaction that appears driven primarily by pH.

2.7 Smart Water EOR

Smart Water EOR aims to use the chemical knowledge of the reservoir to alter the wettability in the reservoir rock by injecting cost-effective brines containing only simple salts which promote the production of hydrocarbons. The injected fluid composition differs from that of the formation water, and is designed to mobilize oil otherwise left untouched.

2.8 Wettability Alteration by Smart Water

In conventional oil production, the produced water is promptly re-injected into the reservoir after it has been separated from the oil in the wellstream. The injection will act as pressure support, but is not able to alter the wettability of the reservoir, as the formation water is already in chemical equilibrium with the rock and oil components of the reservoir. [38] Wettability alteration thus has to come from water injection using a brine with an ionic composition different from that of formation water, which can be achieved by e.g. dilution of the formation water.

When a Smart Water of low salinity is injected in tertiary recovery mode, the water wetness of the rock is likely to increase because of releasing organic material from the clay surfaces. The increased water wetness of the rock causes increased capillary trapping of oil droplets. While this sounds somewhat counter intuitive in the first place, an increase in water wetness also allows the injected water to imbibe into bypassed pores which are not yet flooded, as shown in Figure 11.

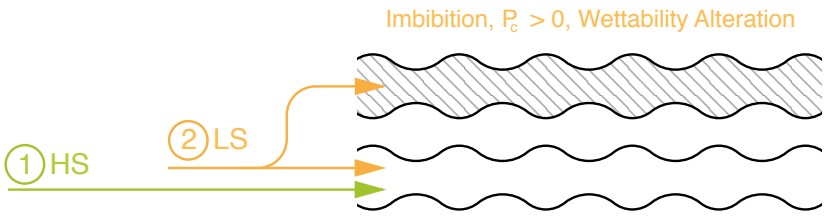

Figure 11: Schematic Illustration of Smart Water Imbibition into Bypassed Pores in a Tertiary Flooding Mode, adapted from Strand *et al.* [35]

The imbibition effect can displace volumes of oil to counter the increased capillary trapping the higher water wetness entails, and if it is possible to mobilize a larger volume of oil from these previously bypassed pores, compared to the volumes that become immobilized through capillary trapping, a net increase in production volume can be extracted from the reservoir—given that a sufficient volume of discrete oil globules coalesce to form a continuous oil phase.

2.8.1 Low Salinity Smart Water Flooding

Being able to increase oil recovery by injecting low-salinity Smart Water brines into the reservoir instead of high-salinity brines such as the original formation water or sea water has been thoroughly documented in experiments. [38–41] Several theories have been suggested to explain this behavior; [42–46]

- Fines Migration
- Impact of Alkaline Flooding
- Multicomponent Ion Exchange (MIE)

- Microscopically Diverted Flow
- Expansion of Double-Layer

Recently, Austad *et al.* [47] proposed another suggestion for the low-salinity Smart Water mechanism, where the desorption of organic material is caused by a local increase in pH at the clay surface due to cationic exchange between adsorbed divalent ions (mainly Ca^{2+}) and H^{+}, which increases the alkalinity of the reservoir fluid. Parallel to this, the increase in pH caused by this rapid cationic substitution can effectively reduce the concentration of the protonated forms of organic material to which subsequently reduces the relative affinity of these organic components toward the clay surface. This also causes the organic material to desorb from the surface. Consequently, the rock surface as a whole becomes more water wet. [48] The suggested release mechanism is presented graphically in Figure 12 and Figure 13 for acidic and basic organic material, respectively.

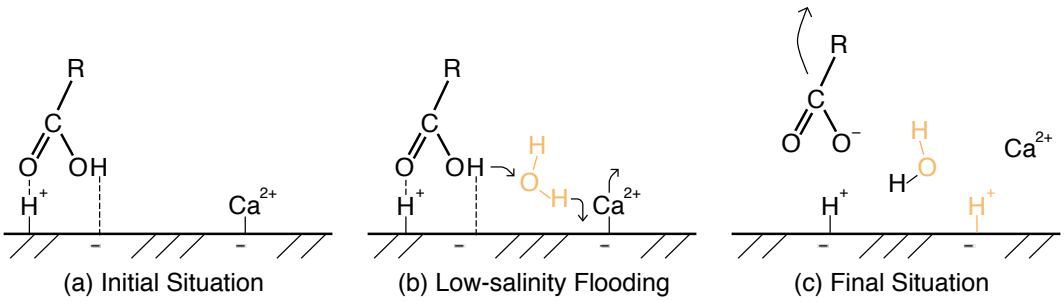

Figure 12: Proposed Mechanism for Acidic Organic Material Desorption from Clay Surface During Low-Salinity Flooding, adapted from Strand *et al.* [35]

If enough oil is released from the clay surface, the possibility of establishing an oil bank of a continuous oil phase arises. The oil bank will then be made up from these released oil globules, and can be displaced toward a producing well. To enhance the oil recovery, the mobilization of oil has to be greater than the volume affected by the increased capillary trapping due to increased water wetness of the rock.

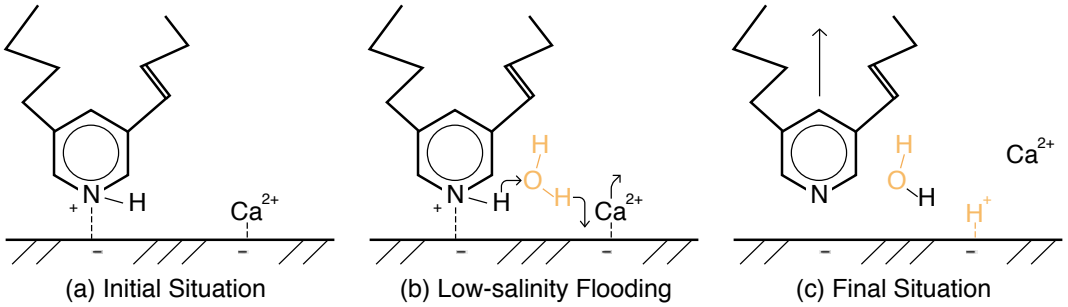

Figure 13: Proposed Mechanism for Basic Organic Material Desorption from Clay Surface During Low-Salinity Flooding, adapted from Strand *et al.* [35]

The reactions can also be described with three chemical equilibria, given in Equations 7–9. Note that the base reaction in Equation 7 is exothermic, which has been determined in temperature sensitivity studies. [48] This corresponds well with the difficulty of low-salinity Smart Water Enhanced Oil Recovery in high-temperature production tests. [49]

$$\text{Clay}{-}\text{Ca}^{2+} + \text{H}_2\text{O} \leftrightharpoons \text{Clay}{-}\text{H}^{+} + \text{Ca}^{2+} + \text{OH}^{-},\ \Delta\text{H} < 0 \tag{7}$$

$$\text{Clay}{-}\text{R}_3\text{NH}^{+} + \text{OH}^{-} \leftrightharpoons \text{Clay} + \text{R}_3\text{N} + \text{H}_2\text{O} \tag{8}$$

$$\text{Clay}{-}\text{R}{-}\text{COOH} + \text{OH}^{-} \leftrightharpoons \text{Clay} + \text{R}{-}\text{COOH} + \text{H}_2\text{O} \tag{9}$$

The presence of calcium precipitates in the formation, such as calcite ($CaCO_3$) and anhydrite ($CaSO_4$), can buffer this effect as free cations are dissolved into the brine, which increases the relative affinity of calcium to the clay surface. Especially so in temperatures over 100 °C, as the hydration energy is lowered drastically, increasing the reactivity of Ca^{2+}. As a result of this, H^+ will be able to desorb less divalent cations from the clay surface.

2.8.2 Wettability Alteration by High-Salinity Flooding

Tang *et al.* [38] have reported substantial increases in recovery when using a high-salinity injection brine in cores with a very low-salinity formation water.

Table 3: High Salinity Recovery Tests in Low Salinity Formation Water Cores. [38] WF and SI denotes Water Flooding and Spontaneous Imbibition experiments, respectively.

Core Name		Connate Salinity	Invading Salinity	Recovery
DG-2	(WF)	1	1	55.2
DG-63	(WF)	0.1	1	63.1
DG-61	(WF)	0.01	1	78.1
DG-2	(SI)	1	1	38.3
DG-62	(SI)	0.1	1	43.5
DG-60	(SI)	0.01	1	47.5

These findings have since been repeated by two studies, where waterflooding of Berea sandstone once again revealed that the ultimate recovery increased in a core with low-saline connate water when using a high-salinity injection water, compared to using a low-salinity injection brine. [50, 51]

When injecting a low-salinity brine, the system becomes more water wet as the organic material is desorbed from the surface due to increased pH. Conversely, injecting a high-salinity brine can cause Ca^{2+} to exchange with H^{+} on the clay surface, which reduces the pH. This reducing in pH increases organic adsorption to the surface and reduces water wetness. Strand *et al.* [35] propose that this mechanism can result in EOR effects given the right conditions, because of decreasing the capillary trapping of oil droplets.

Significant oil recovery from high-salinity flooding is thought to be dependent

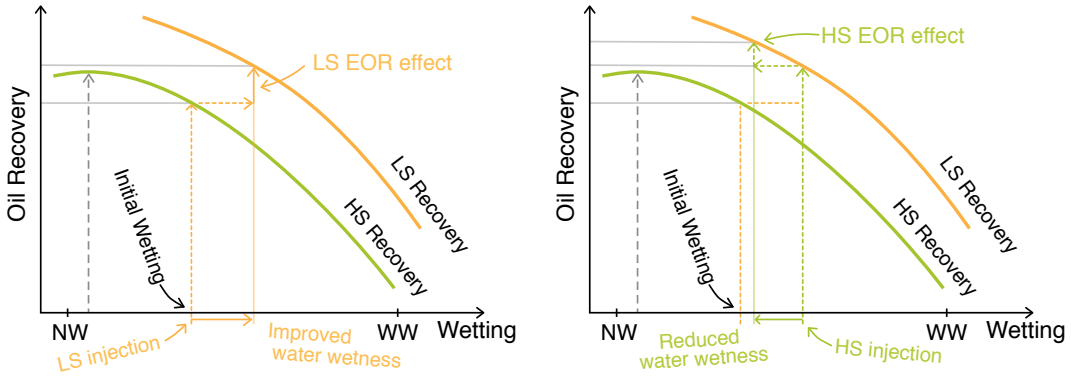

Figure 14: Potential for increased recovery in a high-salinity flood, adapted from Strand *et al.* [35]

on a certain degree of water wetness in the reservoir before the flooding starts. The proposed mechanism for increased recovery is illustrated conceptually in Figure 14. The green, upper curve represents the recovery vs. wettability for a low-salinity flood, whereas the orange, lower curve represents the recovery potential for a high-salinity brine. As the low-salinity brine is injected, the water wetness increases and mobilizes oil from pores which would otherwise be bypassed by using a high-salinity brine. As the water wetness increases, as discussed previously, the capillary trapping of oil increases. To reverse the trapping effect, high-salinity brine is injected and can in theory mobilize more oil due to reducing said capillary effects. The effect is thought to increase as the slope of the low-salinity recovery line steepens.

2.8.3 Slug Injection vs. Continuous Injection

Injecting a slug of low-salinity Smart Water water has been proposed by Seccombe *et al.* [52] The study indicates that a slug with a volume corresponding to 40 % of the pore volume may be sufficient to get the Smart Water benefit of a low-salinity brine throughout the reservoir, accounting for dispersion due to mixing with formation water in the rock between injector and producer. However,

the study is based on a one-Dimensional dispersion model, the accuracy of which has been deemed questionable according to a study comparing one- and two-dimensional dispersion models. [53]. It was shown that the one-dimensional approach possibly could overestimate the incremental oil produced from a large slug, when comparing to two-dimensional simulations deploying a 5-spot pattern.

The conceptual idea of injecting a slug instead of having a continuous low-salinity injection makes perfect sense. It will have three main benefits with regards to field development;

1. Reduction of cost associated with the making of the low-salinity brine for a continuous injection, making it increasingly economically viable
2. Added possibility of secondary wettability alteration by the high-salinity flood which follows the slug of low-salinity brine
3. Possibility of adjusting initial salinity and slug size to optimize project economy

Knowing more about the threshold salinity for low-salinity brines is therefore important with regards to calculating the most cost-efficient injection salinity and slug volume.

3 Methodology and Preparation

The following is an outline of the methodology used for carrying out the experiments themselves and the additional work with regards to chemical analysis which is undertaken during and after flooding procedures.

3.1 Core Material

The three cores used in this experiment originate from the Yme field located offshore Norway in the southern parts of the North Sea. Top of the reservoir is located at a depth of around 3150 m. The coring depth for the cores used is around 3160 m.

The cores wew chosen because of their high clay content, which is necessary for the low-salinity effect to take place. Apart from precipitated anhydrite in the core, due to the reservoir temperature being 110 °C, the cores are relatively clean from a mineralogial point of view. Refer to Table 4 for approximate mineralogical core data from an X-Ray Diffraction analysis of core samples in the same coring interval.

3.2 Crude Oil

The crude oil was supplied by Total, and was chosen because it contains a good amount of active organic material, to promote organic adsorption onto the clay surface during ageing of the core. Refer to the below Table 5 for oil data.

Table 4: Mineralogical Core Data by weight fraction, from XRD analysis.

Mineral	Weight %
Quartz	67.7
Illite / Mica	13.2
Kaolinite	10.7
K-Feldspar	2.9
Plagioclase	2.8
Pyrite	1.2
Siderite	0.5
Calcite	0.4
Dolomite	0.4
Chlorite	0.2

Table 5: Data for the oil used in the experiment

Property	Unit	Value
Acid Number	[KOH/g]	0.1
Base Number	[KOH/g]	1.8
Density	[g cm^{-3}]	0.846
Viscosity	[mPa·s]	17.6

3.3 Viscous Flooding

In the experiments conducted for this thesis work, the cores were flooded using a method called Forced Imbibition, or Viscous Flooding. This means that fluid is forced through the core by applying a differential pressure over the rock sample and allowing brine to pass through the core from a brine reservoir to an effluent

collector. This method is opposed to Spontaneous Imbibition, where the core is left submerged in brine in a pressurized cell for a substantial period of time, where the only forces governing the displacement of oil in the core is of gravitational and capillary nature.

A sketch of the viscous flooding setup is shown in Figure 15. The setup was built around a Hassler core-holder. Such a core-holder is in essence a simple apparatus that, connected to a pressure source, can apply significant confining pressure on the lateral area of the core, forcing fluids to flow through the core axially instead of simply bypassing the core by flowing between the rubber sleeve and the core.

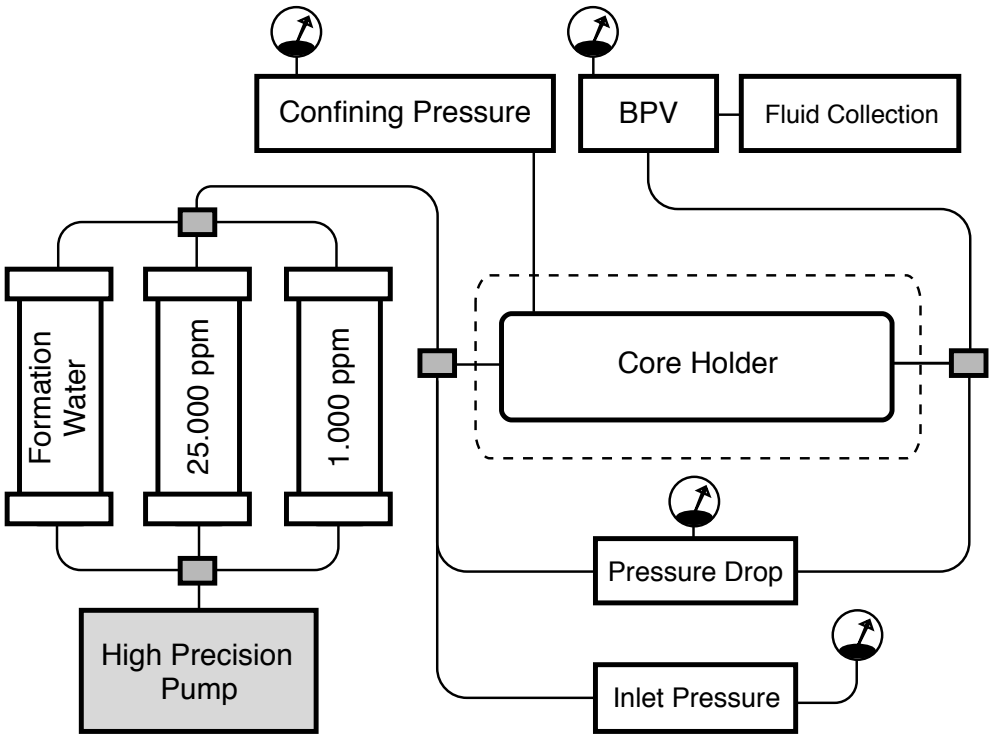

Figure 15: Schematic of the viscous flooding setup. The dashed line represents the heating cabinet boundary.

A back-pressure valve (BPV) at the system fluid outlet facilitated pressurized flooding to avoid having the more volatile components of the oil bubble out while in the core. This was done because a three-phase system is much more complex

compared to a two-phase system, and having gas bubbles in the core during the experiment would have been problematic with regards to the integrity of the experimental results.

3.3.1 Brine Control

The different brines were stored in their respective displacement cells and were connected to the core flooding input via a valve system which allowed for seamless switching of the brine without having to stop and start the pump. This was done to avoid unwanted pressure transients during the flooding process, which can inadvertently mobilize volumes of oil which would not otherwise be mobilized.

3.3.2 Effluent Collection

The effluent was collected in a graded burette. Fluid levels and recovered volumes could then be read directly from the gradations, and the burette also allowed for drainage of the effluent water phase for analysis. In the final production test of Yme-16, a fluid handler was used in conjunction with several graded test tubes. This was done to avoid a recurring problem with the burettes—oil droplets which tended to stick to the glass wall when the burette was drained, making it more difficult to get a correct reading of the produced oil volume.

3.3.3 Viscous Flooding Schedule

All of the cores did not follow the same injection sequence with regards to injected fluid. However, all cores were initially flooded with formation water. Yme-18 was being flooded with medium-saline brine before the low-salinity flood, whereas Yme-19 and Yme-16 were flooded with low-salinity brine immediately after the formation water.

All of the cores were flooded with formation water following the low-salinity flood to see whether the cores responded to a secondary wettability alteration by high-salinity flooding. Refer to Table 6 for the flooding schedule for the three cores. The cores were flooded with a rate equal to 4 pore volumes/day, in all stages of flooding.

Table 6: Core Flooding Sequences

Core Name	Yme-18	Yme-19	Yme-16
Primary	FW	FW	FW
Secondary	25.000 ppm	1.000 ppm	1.000 ppm
Tertiary	1.000 ppm	FW	FW
Quaternary	FW	—	—
Flooding Rate	4 Pore Volumes/day		
Temperature	60 °C		

3.4 Effluent Analysis

To gain a better understanding of the underlying chemistry of the results in the experiments, several effluent samples were analyzed by ion chromatography, pH- and density metering.

3.4.1 Ion Chromatography

To analyze the chemical composition of the effluent samples, an ion chromatograph is used. The make and model of the ion chromatography stack is *Dionex ICS-3000*. All samples were diluted 200 times and the ion chromatography response compared to the response of diluted standards with known concentrations of the ions of interest. Dilution was handled by a syringe

pump liquid handling setup by *Gilson*.

Originally, only a few samples were to be analyzed. However, during the flooding of Yme-16, it was decided to do a more extensive analysis of the effluent samples from the Yme-16 and Yme-19 floods. Regrettably, some of the samples had already been discarded and naturally could not be analyzed. The remaining samples were to be analyzed in the IC.

3.4.2 pH-Measurements

pH-measurements were carried out as soon as possible after collection, to avoid contamination associated with the brine equilibriating with atmospheric CO_2, which can sour the sample. The pH-value was measured using a *Mettler Toledo SevenCompact* with a *Mettler Toledo inLab Semi-Micro* pH sonde.

3.4.3 Density Measurements

The effluent density was measured in conjunction with pH to determine which brine mix is at the fluid outlet of the core, which allows the immediate recognition of whether or not the effluent is transitioning between two different injection brines. The density was measured using an *Anton Paar DMA 4500 Density Meter*.

3.4.4 Chemical Simulation

While not a major part of the thesis, static chemical simulation will be used in an attempt to determine potential sources of ions and solubility of different substances in the different NaCl brines. A specific software, called *PHREEQC*, will be used for these simulations.

3.5 Brine Preparation

Brines are simply different salt water solutions. For our experiments, different brines have to be mixed according to desired chemical properties.

Mixing of brines is a matter of precision which includes careful measurement of salts and volumes, stirring, filtering and finally proper storage to ensure chemical integrity of the brine.

High saline brines are prepared by dissolving each salt separately in flasks and subsequently combining the separate brines into a larger stirring flask for mixing. This has proven to be better in avoiding precipitation compared to dissolving all the salts in a single flask.

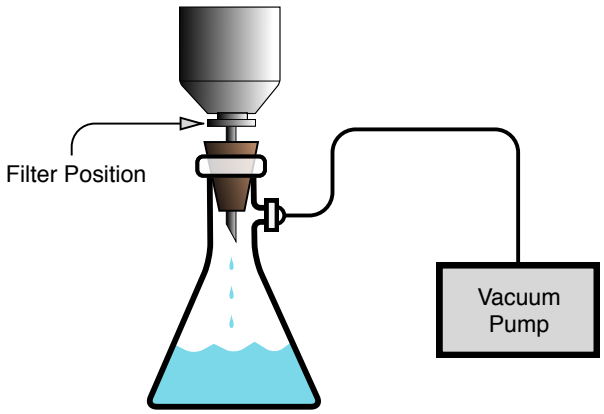

Figure 16: Schematic of apparatus used for brine filtering

When the brine has finished mixing, it has to be filtrated for any possible particles of hair or dust in the water, which can block pore throats in the core. Reducing the core quality is obviously not good for the integrity of the experiment. All brines are therefore filtrated using a 0.22 µm filter to remove any impurities in the brine following the mixing stage.

The filtering setup, seen in Figure 16, consists of a vacuum pump, a Büchner flask and a two-piece filtering funnel connected to the flask via a black elastomer adapter, to ensure a good seal. In between the two pieces of the funnel, which are latched together with a grip, it is possible to place a micro-filter. The brine is

sucked through the filter by the vacuum pump, filling the flask with filtered brine.

After filtering, the brines are stored in air tight flasks, out of the sun.

3.5.1 Brine Composition and Data

The ionic composition and brine properties are listed in the below Table 7. The composition of the salts are given in terms of ionic concentration.

Table 7: Chemical Composition of Brines

Brine:	FW	25.000 ppm	1.000 ppm
Na^+ [mmol L^{-1}]	1540	427	17
Ca^{2+} [mmol L^{-1}]	90	0	0
Cl^- [mmol L^{-1}]	1720	427	17
TDS [g L^{-1}]	103.25	25	1
Density [g cm^{-3}]	1.06544	1.01553	0.99907
pH	5.33	5.63	5.82

3.6 Core Preparation

The three different cores used in these experiments were prepared using more or less the same procedure to allow for comparable results. The goal of core preparation is to ready the core samples for the experiments while preserving the original properties of the actual reservoir rock.

First and foremost, the cores which arrive crudely cut from the original reservoir core have to be cut into cylindrical specimens to facilitate insertion of cores into the Hassler core-holders used in the experiments. This is done using a specialized diamond cutter with a large, heavy blade for precise, clean cuts with minimal chipping. Core-holders are used for all flooding purposes in the

preparation stages

The different stages of the core preparation process are outlined in the following sections.

3.6.1 Core Cleaning

Traditionally, cores have been chemically cleaned by alternately injecting aggressive solvents, for example toluene and methanol. [7] These chemicals have a tendency to release and remove polar hydrocarbon components adsorbed on the rock surface, which can change the core wettability. To best preserve the original rock properties, the cores were therefore cleaned using a mild cleaning procedure, carried out in five steps;

1. **Initial Flooding with High Saline Formation Water**

Initially the core is flushed with formation water to introduce moisture and stabilize the specimen after a long period of storage. This also allows a quasi-quantitative measuring of the anhydrite ($CaSO_4$) concentration in the effluent, as to indicate how long we must expect to clean the core in Step 4 of the cleaning process. The actual formation water used in this experiment was not of the same composition as formation water found in the reservoir where the cores were sampled. This is of little experimental importance. The formation water was, however, the same brine which was used as a reference fluid during the experiments.

2. **Removing Oil Components by Kerosene Flood**

Kerosene is used to displace the pore content of the core with minimal rock surface interaction. Flooding with kerosene, instead of the traditional methanol/toluene cleaning, better preserves the original wetting conditions of the core sample, ensuring a better representation of the actual subsurface

conditions. This is because a larger amount of the polar components are allowed to stay on the rock surface during the flood. Several pore volumes of kerosene is injected, until the effluent is acceptably clear, indicating that the core is ready for the last step of the cleaning process. If two successive effluent samples share the shame color hue, the kerosene flooding is stopped.

3. Flushing with Heptane

The cores were flushed with about two pore volumes of heptane after completion of the kerosene injection. This completely removes kerosene from the core, with minimal impact on the wetting conditions and polar components present on the rock surface.

4. Final Flooding with Low-Salinity Brine

The cores used in these experiments contained significant amounts of anhydrite. This necessitates a final flooding stage in the cleaning process, where the cores were flooded with large amounts of water to allow for the dissociation and subsequent removal of the sulfate. Low-salinity brine was used in lieu of distilled water to inhibit clay swelling in the core. Composition of this low-salinity water was simply 1.000 ppm NaCl.

Yme-18 and Yme-19 cores were flooded with a very large amount of water, upwards of 200 pore volumes. At this point, it was necessary to abort the removal of anhydrite regardless of the sulfate concentration in the effluent, to avoid destroying the core material.

The Yme-16 core was *not* flooded with low-salinity water at length, but rather only flooded sufficiently to displace the heptane before drying. This was done in order to be able to compare the production tests of Yme-19 and Yme-16, to see the effect of having a high anhydrite presence in the core.

5. Core drying

At the end of all flooding processes, the core is placed in a heating cabinet at 90 °C. A high temperature environment allows for faster evaporation of remaining liquids in the core, readying it for further preparation. The core is dried in the heating cabinet until it weighs the same on two successive weighings, indicating that all the fluids have been evaporated.

3.6.2 Fluid Saturation

Saturating the core with initial fluids required by the experiment is akin to the cleaning process in that it is also a time consuming multi-stage process.

1. Saturating Core With Diluted Formation Water

The core is first placed resting on marbles inside a plastic container in a small sealed chamber. Air is then evacuated from the chamber using a vacuum pump, before the diluted formation water is fed through a valve, until the core is fully submerged. This allows the diluted formation water to enter the core without having to displace an already present gas phase. Refer to Figure 17 for a setup schematic of the saturation apparatus. Formation water dilution must comply with the relation given in the following Equation 10;

$$C_{\mathrm{DFW}} = C_{\mathrm{FW}} \times S_{\mathrm{wi}} \tag{10}$$

Where C_{DFW} is the salinity of the diluted formation water, C_{FW} is the salinity of the formation water and S_{wi} is the initial water saturation given as a fraction of the pore volume.

For simplicity, one can also assume that a certain residual water saturation, S_{wi} is desired in the core. Then we can express a factor f the following way;

$$S_{wi} = \frac{1}{f} \tag{11}$$

The formation water will then have to be diluted f times, volume for volume. For the set of experiments in this project, the formation water was diluted to one fifth of initial salinity, so as to cater for an initial water saturation of $S_{wi} = 0.20$. The dilution is necessary for achieving the correct formation water salinity in the residual water of the core.

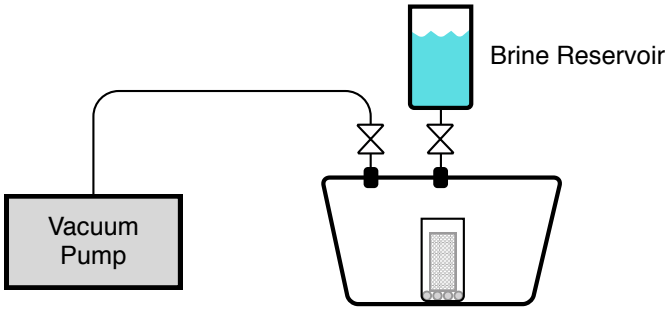

Figure 17: Schematic of apparatus used to introduce water to the core.

2. Establishing Residual Water Saturation

Following the complete water saturation of the core, it is placed inside a desiccator to enhance water evaporation. Evaporation is catalyzed by the desiccant, usually dried silica grains, which adsorb moisture and decrease the air humidity within the desiccator, increasing the rate of evaporation. By controlling the amount of silica and the rate of which it is introduced into the desiccator, the rate of evaporation can to some extent be controlled.

The desiccation process has been proven effective at creating uniform water saturation profiles in the cores, where equilibriation takes place in very short time. [54] Chemical equilibriation takes longer to achieve, especially with a two-phase liquid in the plug (such as after the core has been oil saturated) because of reduced mobility in the liquid phases.

Desiccation is stopped once the core reaches its target weight, which is calculated with the below Equation 12.

$$W_{\mathrm{T,S_{wi}}} = \left(W_{\mathrm{Wet}} - W_{\mathrm{Dry}}\right) \times S_{\mathrm{wi}} + W_{\mathrm{Dry}} \tag{12}$$

Where $W_{\mathrm{T,S_{wi}}}$ is the target weight of the core at desired initial water saturation, W_{Wet} is the weight of the core when saturated with water, W_{Dry} is the dry weight of the core and S_{wi} is, as before, the initial water saturation as a fraction of the pore volume. After the initial water saturation is established, the core is left to equilibriate in a small container over night. This is done because the water evaporates from the outside and in, which means that the core will be more wet in the center compared to near the surface. Resting the core will cause the remaining water to settle outwards, promoting a more linear saturation profile in the core.

3. Saturating Core with Oil

Since Hassler core-holders are used for oil saturation, the saturation setup is very similar to the viscous flooding setup shown in Figure 15. In fact, the concept is the exact same—except that the oil will be flooded through the core in both axial directions to ensure a fully saturated core. Similar to the viscous flooding setup, the core is placed in the core holder where a confining pressure of 2 MPa is applied, and the core holder is in turn placed inside a heating cabinet at 50 °C. The lines are evacuated of air using a vacuum pump to avoid air bubbles in the core after saturation. The pressure is kept above the partial pressure of water to avoid evaporation of water in the core and subsequently an increase in formation water salinity. The oil is then injected with 2 pore volumes in each direction, to ensure maximum saturation is achieved. Before the next step, the core is allowed to cool down to avoid evaporation of volatile components from the oil in the core.

Refer to Figure 18 for a setup schematic of the saturation apparatus.

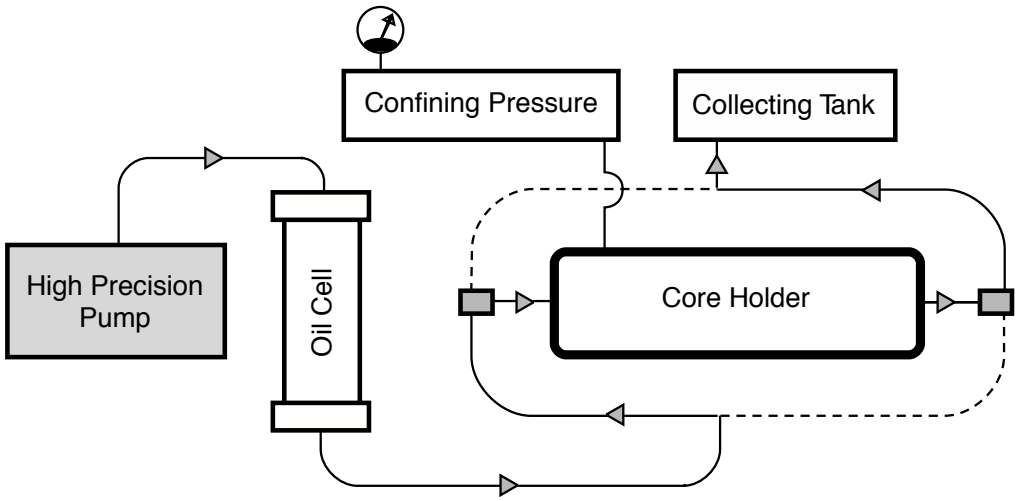

Figure 18: Schematic of apparatus used to introduce oil to the core.

3.6.3 Core Maturation

When the core has been fully saturated with oil and water, chemical equilibriation must be achieved. To facilitate this, the saturated cores are wrapped in teflon tape and put into maturation cells where the core is submerged in the same crude oil the core is saturated with.

The cells are sealed and put into heating cabinets at 60 °C for two weeks.

Increased temperature helps speed up the equilibriation process. It is also of importance that the experiments are being carried out in temperatures far above room temperature. During maturation, polar components will attach to the rock surface, and the homogeneity in core chemistry is enhanced.

3.6.4 Core Data

All core data collected during the preparation of the cores are listed in Table 8.

Table 8: Physical Core Data

Core Name:	Yme-18	Yme-19	Yme-16
Length [cm]	7.21	6.42	7.30
Diameter [cm]	3.78	3.78	3.78
Bulk Volume [cm^3]	80.91	72.05	81.92
Dry Weight [g]	178.57	161.33	179.01
Wet Weight [g]	191.40	171.35	191.35
Target Weight [g]	181.14	163.34	181.57
Pore Volume [cm^3]	12.67	9.90	12.19
Porosity [%]	15.66	13.73	14.88
Permeability [mD]	370–400	270–300	460–490

Length and Diameter are simply measured using a regular caliper after the cores have been cut into cylindrical specimens.

Dry weight is recorded after the core has been cleaned and dried, using a scale. The wet weight is recorded using the same scale after the core has been saturated with diluted formation water. The difference between the dry- and wet weight of the core can be used in conjunction with the density of the diluted formation water, ρ_{DFW}, to calculate the effective pore volume of the core, using Equation 13.

$$PV_{\mathrm{E}} = \frac{W_{\mathrm{Wet}} - W_{\mathrm{Dry}}}{\rho_{\mathrm{DFW}}} \tag{13}$$

Effective porosity of the core, is calculated using Equation 14, where V_{Bulk} is the core bulk volume and ϕ_{E} is the effective porosity as a fraction of the core bulk volume.

$$\phi_E = \frac{PV_E}{V_{Bulk}} \tag{14}$$

Permeability is calculated using Darcy's Equation as seen in Equation 15, where the differential pressure over the core, ΔP was measured during the 1.000 ppm water flood at steady state with controlled flow rates.

$$Q = -\frac{kA}{\mu} \times \frac{\Delta P}{L} \tag{15}$$

The other parameters of this equation are the volumetric flow rate, Q, the cross-sectional area of the core, A, the length of the core, L, the viscosity of the fluid, μ, and finally k denoting the permeability of the core.

4 Results

4.1 Yme-18 Core Flooding Results

4.1.1 Oil Production Test, Temperature at 60 °C

The following Figure 19 shows the production data from the oil production test of Yme-18. Initial recovery with the formation water flood was a bit over 49 %OOIP. There was no additional recovery during the 25.000 ppm flood and, similarly, the absence of production suggests no indication of secondary wettability alteration during the last formation fater flood. The 1.000 ppm low-salinity flood improved the recovery by roughly 4 %OOIP.

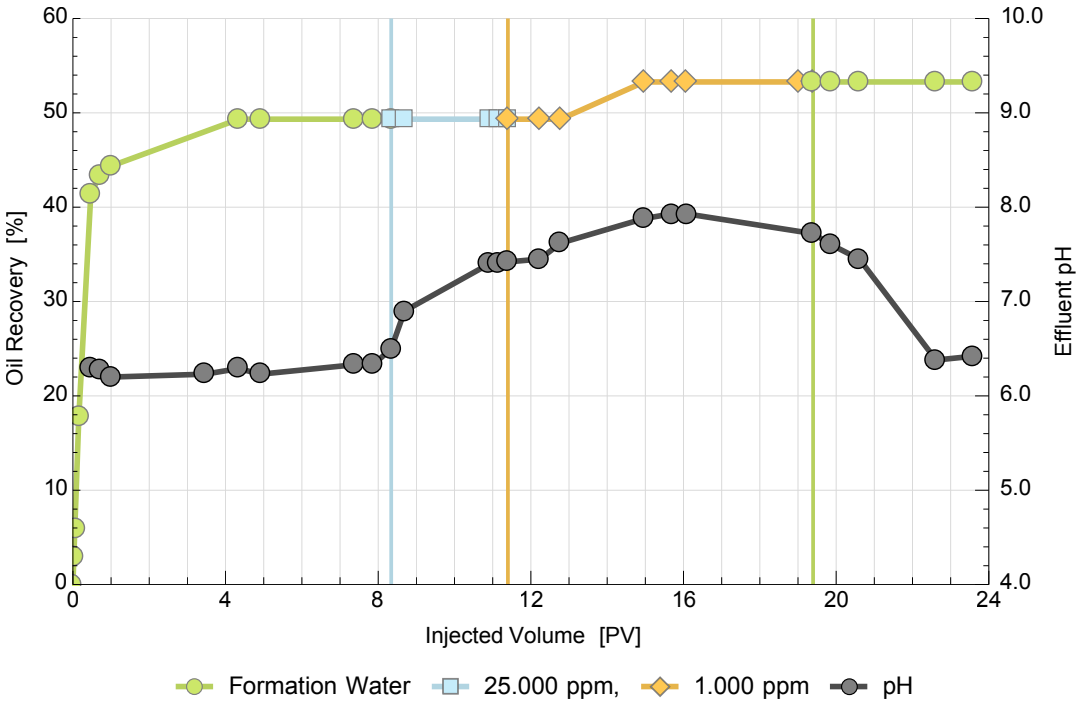

Figure 19: Yme-18 Oil Production Test, pH measured at 25 °C

Initial effluent pH comes out at about 6.25 units. The pH stabilized at the end of the 25.000 ppm flood, at 7.5 pH units. However, the alkalinity of the brine increased further after starting the injection of the 1.000 ppm brine, peaking at a value just below 8 pH units. The difference between the initial pH and the highest recorded pH is roughly 1.75 units. The pH appears to drop toward the end

of the 1.000 ppm flood, but this could be due to the sample equilibriating with CO_2 overnight, souring the reading. After the injection brine is switched back to formation water, the pH levels return to the levels seen in the previous formation water flood.

4.1.2 Chemical Analysis

The chemical analysis of the Yme-18 core effluent was not extensive. Figure 20 shows the analysis of four samples comparing sulfate and calcium concentrations in the effluent when flooding 25.000 ppm and 1.000 ppm brines.

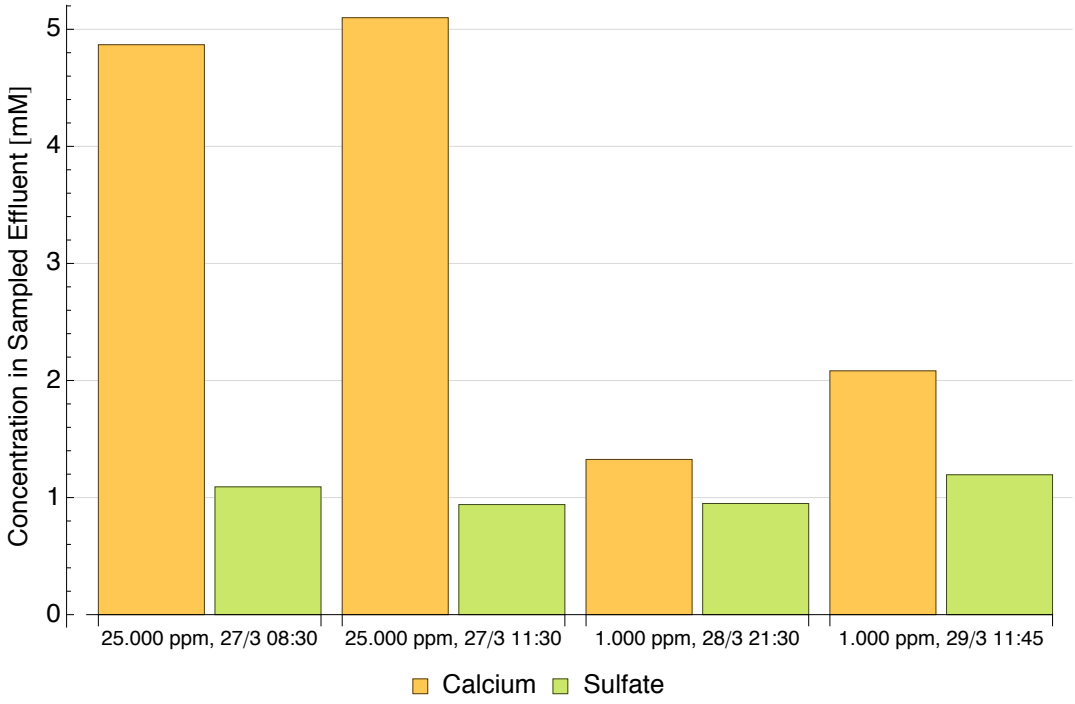

Figure 20: Yme-18 Effluent Analysis.

Sulfate levels were more or less constant during both the 25.000 ppm and 1.000 ppm flood, concentrations hovering around 1 mmol L^{-1}. Calcium levels during the 25.000 ppm flood were between 4.5–5 mmol L^{-1}, whereas during the 1.000 ppm flood the concentration dropped significantly, values staying between 1–2 mmol L^{-1}.

4.2 Yme-19 Core Flooding Results

4.2.1 Oil Production Test, Temperature at 60 °C

The below Figure 21 shows the production data from the oil production test of Yme-19. Initial recovery with the formation water flood was 49 %OOIP. The 1.000 ppm flood increased the oil recovery by about 2.5 %OOIP. A small additional recovery is recorded after switching back to formation water, roughly 0.6 %OOIP.

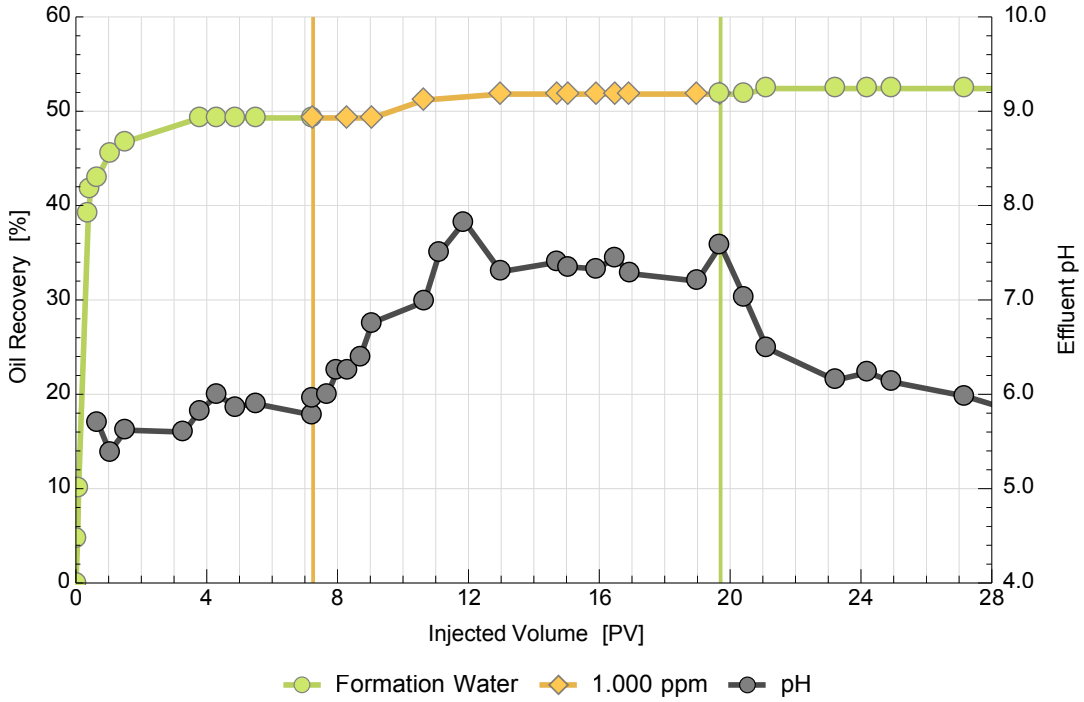

Figure 21: Yme-19 Oil Production Test, pH measured at 25 °C

Initial effluent pH is recorded at roughly 5.65 units. The pH-curve is somewhat dome-shaped and peaks at just below 8 pH units for an apparently very short period, but is on average closer to 7.35 pH units. The differential pH is therefore averaged out to about 1.7 pH units. During the final formation water flood, the pH drops gradually.

4.2.2 Chemical Analysis

As mentioned in Section 3.4.1, several samples from the Yme-19 flood were discarded before the decision was made to do a more extensive chemical analysis on the samples of effluent collected during the flooding. The results of the analysis of all remaining effluent samples are presented in the below Figure 22. The analysis was run to determine the concentrations of calcium and sulfate in the effluent and how they fluctuated during the flooding process.

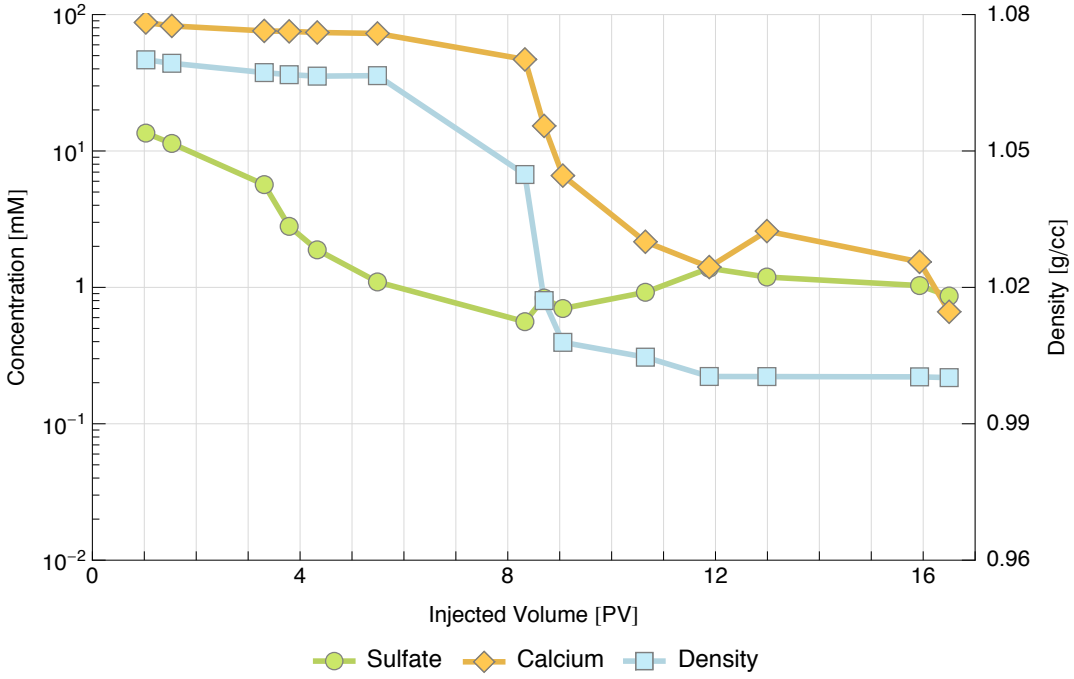

Figure 22: Yme-19 Ion Chromatography Chart.

As the density drops, the effluent transitions from formation water to 1.000 ppm brine. During the fluid transition, the sulfate concentration appears to deflect upwards from a previous downward trend, creating a doming concentration curve. As expected, the concentration of calcium drops heavily as the injection brine transitions from the calcium rich formation water to the completely calcium free 1.000 ppm brine, however the concentration follows a slightly dome-shaped curve in the region between 12 and 16 PV.

4.3 Yme-16 Core Flooding Results

4.3.1 Oil Production Test, Temperature at 60 °C

Figure 23 shows the production data from the oil production test of Yme-16. Initial recovery with the formation water flood was just shy of 49 %OOIP. The 1.000 ppm flood increases recovery by 2 %OOIP. A small additional recovery of 0.8 %OOIP is seen during the second formation water flood.

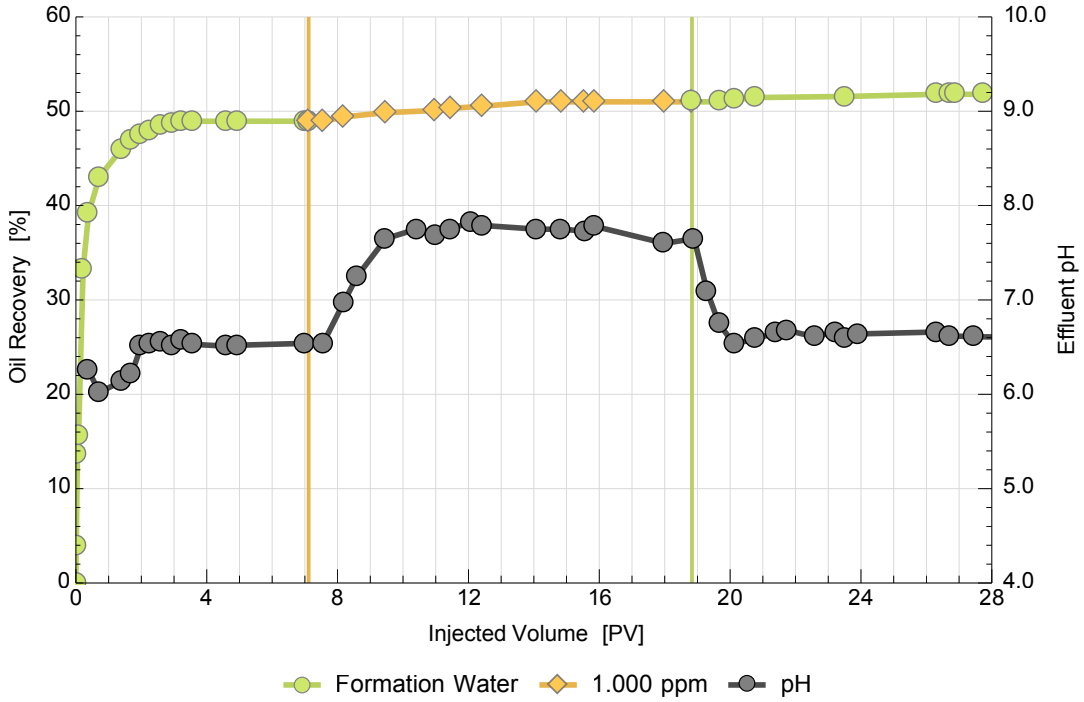

Figure 23: Yme-16 Oil Production Test, pH measured at 25 °C

The very initial effluent pH is trough-shaped, but stabilizes at 6.5 pH units, possibly an effect of substantial oil production during this period. The pH-curve during the 1.000 ppm flooding is very clean, stable around 7.75 units. The differential pH then ends up at 1.25 pH units. The second formation water flood drops the pH quickly to a level a bit above that of the initial flood; roughly 6.6 pH units.

4.3.2 Chemical Analysis

Samples of the initial Yme-16 formation water flood were also discarded before the decision was made to do a more extensive chemical analysis of the effluent from this flooding process. Preferably, some samples of the formation water flood that preceded the transitional period to the 1.000 ppm injection would also be present in the extended analysis.

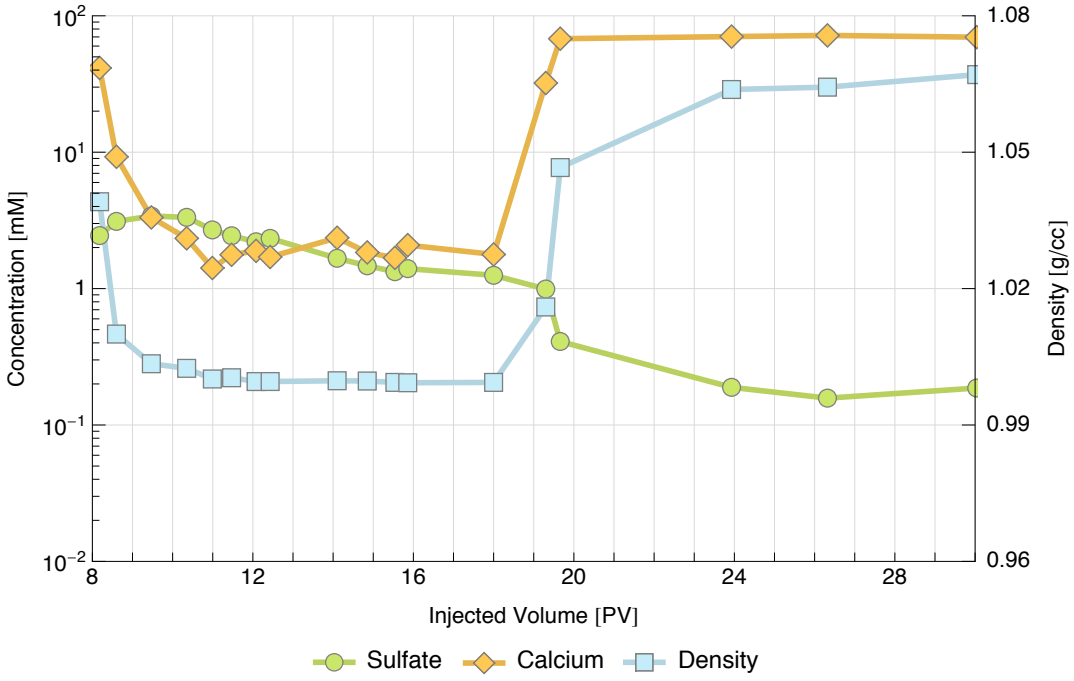

Figure 24: Yme-16 Ion Chromatography Chart.

As the injection brine transitions from formation water to 1.000 ppm NaCl, the calcium concentrations decrease substantially as expected. A dome-shaped curve after completion of fluid transition is present in the data. Sulfate levels appear to be increasing as the transition takes place, but is overall on a downward trend. The concentration clearly drops as the brine transitions back to formation water.

5 Discussion

5.1 Yme-18: Medium-salinity Flood Viability

Yme-18 was flooded with upwards of 200 pore volumes of 1.000 ppm NaCl before the core was saturated and matured. This was done in an effort to relieve the core of its anhydrite content, but this proved only to reduce the amount of anhydrite substantially, but not to actually remove the anhydrite, as evident from the chemical analysis of the 1.000 ppm samples during flooding as shown in Figure 20.

From Figure 20, the chemical analysis of effluent samples taken from both the 25.000 ppm and 1.000 ppm flood show elevated calcium concentrations in the effluent during the 25.000 ppm flood.

These elevated calcium concentrations seen in conjunction with the relatively steady concentration of sulfate during both floods, indicate that calcium is dissolved into the flood at a faster rate when flooding with a 25.000 ppm brine.

We recall, per table Table 7, that the 25.000 ppm brine itself does not contain any calcium, it is composed of only NaCl, the additional calcium has to come from inside the core itself, through a mechanism which is not as active during the 1.000 ppm flood. This leaves us with four possibilities for the sulfate levels in the samples;

- Dissolution of previously precipitated calcium salts other than $CaSO_4$
- Cationic Exchange on the clay surface
- Impurities in the mixing salts
- Impurities in sample glasses

One possible source of dissolution is from calcite cement, which appears in sandstones frequently. We recall the information displayed in Figure 9, which indicates that the concentration of aqueous calcium is likely to be much greater

in a brine with a salinity of 25.000 ppm compared to the case with salinity at 1.000 ppm. However, the same analysis also suggests that the dissolution and concentration of sulfate should also increase, along with the calcium, when flooding with a 25.000 ppm brine. Additionally, the ion chromatography testing did not show elevated carbonate levels, suggesting that calcite dissolution is not contributing to the increased calcium concentration.

The salts used in the brine mixing have a reported potassium impurity level of 5 times that of calcium, and the ion chromatography did not reveal any significant potassium content in the samples. Impurities in the mixing salts are therefore not very likely at all to have contributed to the increased calcium concentration.

The low fluctuation of sulfate in the effluent can possibly stem from the lack of chemical equilibrium in the flooding process. The brine is completely refreshed every 6 hours, which can be much too quickly for a chemical equilibrium to establish. It is fair to assume that the rate of dissolution slows over time, with a value converging to the theoretical equilibrium value as time approaches some arbitrary, large value. It can therefore be argued that the 25.000 ppm brine has a higher equilibriated concentration potential, but that in the given flooding processes, the anhydrite rate of dissolution is limited by the liquid throughput and reaction time, rather than the salinity of the brine.

Impurities in the sample glasses is not very likely, given that the only two glasses containing these apparent impurities happen to be used for the same type of brine effluent, and that they seem to be spiked only with Ca^{2+}.

An alternative that seems increasingly likely with regards to the available data is that cationic exchange on the clay surface is a source of the increased calcium levels in the 25.000 ppm effluent.

When flooding with the 25.000 ppm brine, the relative concentration of sodium ions, Na^{+}, to calcium ions is quite large. Recalling that the surface affinity is controlled amongst other things by the relative concentration of cations in the

brine, it is possible that the sodium ions are replacing some the calcium ions on the negative sites of the clay surface, thus increasing the calcium concentration in the effluent.

The effluent pH increases as the H^+ ions are displacing Na^+ on the clay surface, until an equilibrium is reached. The increased adsorption of sodium ions buffers the system pH—because it competes more strongly with H^+—pH being the main property responsible for the release of acidic and basic material from the clay surface and subsequently the oil recovery is not increased. This can possibly be because the pH has not increased enough compared to the initial flooding pH with formation water to cater for sufficient organic desorption to allow a continuous oil phase to establish.

In the case of the Yme-18 system, the critical point for establishing a continuous oil phase is roughly somewhere between 7.5 and 8 pH units.

When the injection brine is switched from 25.000 ppm to 1.000 ppm, the relative concentration of Na^+ drops drastically, and subsequently, so does the surface affinity and competing strength of the cation. Now the reactivity of H^+ increases in potency which allows for enhanced adsorption of active hydrogen. The pH therefore decreases further, as the equilibrium is pushed toward a more alkaline brine as the concentration of H^+ is lowered.

After a certain exchange equilibrium has established with the new brine in the formation, the water wetness of the rock increases to a critical value following the desorption of more organic material. The oil may then establish a continuous phase which allows the phase to flow and be produced. This value is probably dependent on the micro-structure and mineralogy of the rock, and the viscosity of the oil, as the critical saturation for oil flow is dependent on both capillary and viscous forces.

As a result of the increase in pH following the 1.000 ppm flood, sufficient amounts of oil globules are released and form a continuous phase such that it can

be displaced. An increased production of 4 %OOIP is observed. The Smart Water effect seen in the core is important because it indicates that the core is susceptible to such effects, if the properties of the brine are able to induce them—which the 25.000 ppm brine proved unable. Sadly, the specifics of how the 1.000 ppm changes the system chemistry is extremely hard to discuss given the choice of not analyzing a full suite of effluent samples.

The sum of this discussion is that the 25.000 ppm NaCl brine was not able to mobilize oil to such a degree that it becomes continuous and can be displaced by the injection process. From the Yme-18 experiment it can be argued that in the given crude oil/rock system, a 25.000 ppm flood carried very little, if any, potential. However, the 1.000 ppm brine is able to alter the system chemistry such that oil can be produced. Likely, some threshold exists below which one can improve oil recovery, and for the discussed system this threshold clearly lies somewhere between 25.000 ppm and 1.000 ppm. But where is the low-salinity Smart Water threshold? Project economy can be more beneficial if it is not necessary to produce water with salinities as low as 1.000 ppm—finding this threshold seems critical to optimize project economy.

5.2 Yme-19 and Yme-16

5.2.1 Effect of Anhydrite on the Smart Water Effect

Even though the Yme-19 core was flooded extensively with 1.000 ppm brine in the cleaning stage in an effort to reduce the amount of anhydrite in the core, there is still a significant amount in the effluent. There is reason to believe that depleting the core entirely of anhydrite is a slow and tedious exercise in futility. The analysis carried out on the effluent samples do suggest, however, that the anhydrite content is somewhat higher in Yme-16 compared to Yme-19. This can be visually confirmed in the low-salinity intervals of Figure 22 and Figure 24.

Calculations using the production data show that the period of pure 1.000 ppm flood averages a sulfate concentration in the IC analyses of 1.87 mmol L^{-1} against 1.12 mmol L^{-1}, for Yme-16 and Yme-19, respectively. The attempted depletion appears to have at least lowered the concentration to a relatively smaller amount.

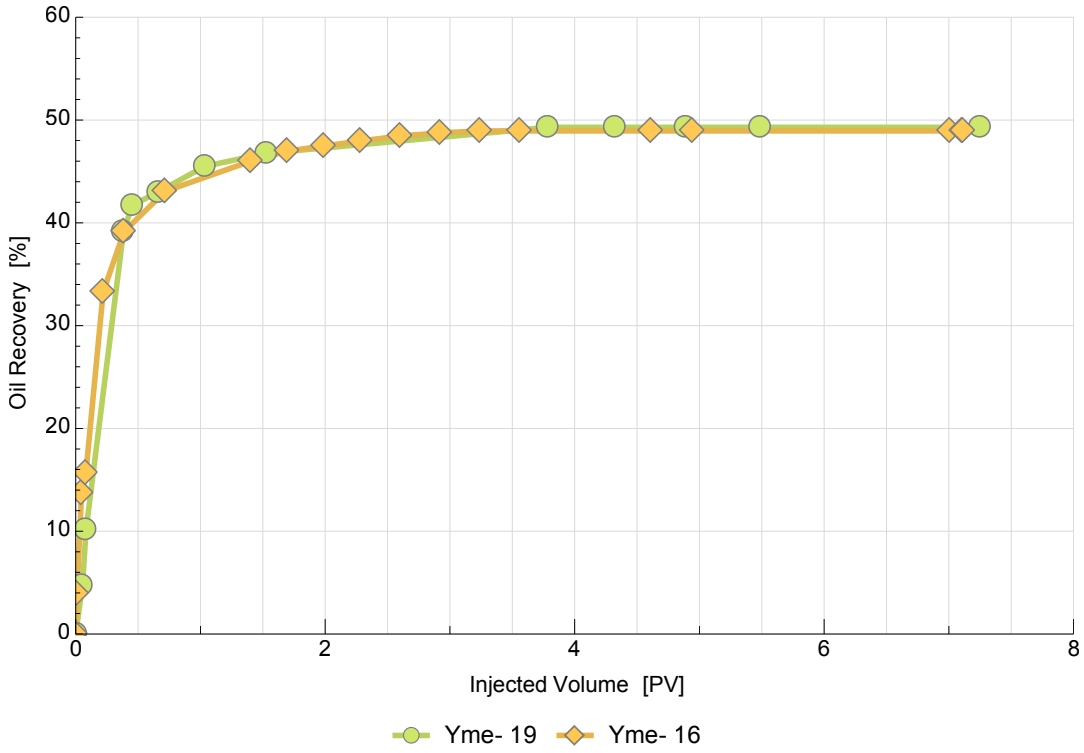

Figure 25: Comparison of oil recovery for Yme-19 and Yme-16 cores, during initial flooding using formation water.

The first impressions of the production test results is that the two cores are quite homogeneous with respect to each other, both reaching an oil recovery close to 49 %OOIP using formation water as a displacing fluid. The production curves from both the Yme-19 and Yme-16 cores during the initial flood is shown in Figure 25. The striking similarities of the production during initial injection can help lower the uncertainties of the differences in produced volumes at later stages. Curve congruency suggest similar wetting properties in the two cores. Also, the deviation from piston-like displacement curves suggest mixed-wet systems in the two cores.

In both cases, as seen in Figure 22 and Figure 24, the concentration of calcium

and sulfate converge in the low-salinity interval—implying that the dissolution of anhydrite is the only source of calcium, which is to be expected in light of the discussion of Yme-18.

The relative concentration of Na^+ in the core during the 1.000 ppm brine flood is not high enough for sodium cations to effectively displace large amounts of Ca^{2+} from the clay surface, which means that the surface equilibrium is only a battle between Ca^{2+}, H^+, the active organic components, and their relative replacement power. The apparent increase in sulfate concentration during low-salinity flooding is most likely an effect caused by the large salinity gradient—the high-salinity formation water lowers the solubility of anhydrite.

As evident by the data, a Smart Water effect is seen in both cores during the 1.000 ppm flooding. The low additional recovery of 2–2.5 %OOIP suggests that the effect is dampened by the dissolution of free calcium from the precipitated anhydrite in the core. This is much below what we would expect in an ideal case of injecting low-salinity Smart Water, which can be upwards of 10 %OOIP. [35]

As the concentration of Ca^{2+} in the brine is kept more or less constant because of the dissolution of anhydrite, the relative replacing power of calcium stays high, which prevents its displacement by H^+, effectively buffering the pH.

Both cores produce additional volumes during the low-salinity flood after the pH of the effluent crosses a threshold value of somewhere just below 7 pH units—regardless of the initial effluent pH, which is somewhat more acidic in Yme-19. Attempting to determine this critical pH-threshold would be very interesting, such as injecting successive floods of lower and lower salinity brines until oil is produced.

The difference in additional produced oil during the low-salinity flood is within the margin of error in experiments such as these, due to large uncertainties in recording the produced oil volume. However, because of the astounding similarity in the initial recovery curves, I choose to justify a comparison in spite of

the associated uncertainties.

Yme-19 has a more acidic initial effluent pH compared to Yme-16. A more acidic environment, with a pH closer to the optimal 5 units, should allow more organic material to adsorb to the clay surface during ageing of the core. The average pH during the low-salinity plateau is actually higher in Yme-16, but the absolute pH gradient from formation water injection to low-salinity injection is slightly greater in Yme-19. Together with the slightly lower amount of calcium dissolution during the flooding in the Yme-19 core, this can give a reasonable explanation for the additional recovery.

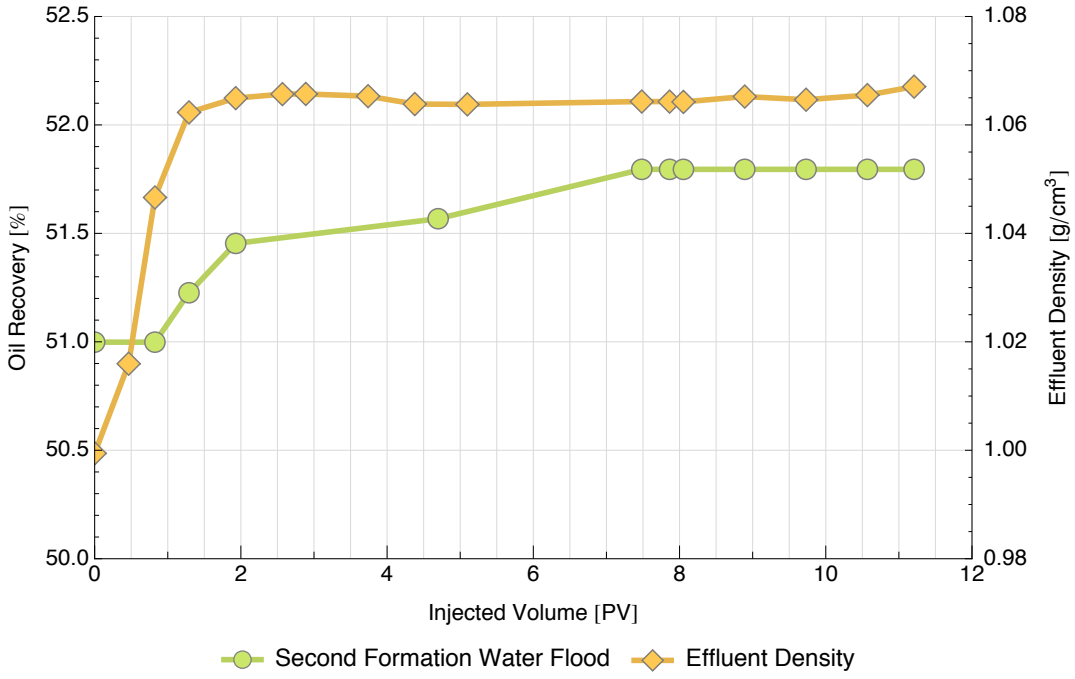

Figure 26: A closer look of the second formation water injection in the Yme-16 core, injected volumes normalized to the time of switching.

5.2.2 Secondary Wettability Alteration

During the final flood with formation water, both cores respond with a slight increase in recovery. Looking closer at the data, such as in Figure 26, it is revealed that the density of the fluid increases before the breakthrough of the additional oil. This is an indication that the oil was not released by a pressure gradient in

the reservoir related to the opening and closing of valves when switching brines, seeing as oil released from a pressure effect would be expected in the effluent much earlier. This could therefore be an effect introduced by the salinity gradient.

The very small additional volume cannot be said to be a definitive result of secondary wettability alteration, however, it is an *indication* that such changes in wettability possibly have occured in the cores. During the second formation water flood, the pH in both cores drop significantly, and approach the values seen in the initial formation water flood—entirely as expected.

A large volume of increased recovery is not expected in this core material if the mixed-wet nature of the cores during the initial formation water floods are taken into account. This is consistent with the theory outlined by Strand *et al.* They propose that the wetting conditions have to be more or less strongly water wet to successfully extract significant volumes from reduction of the capillary trapping.

5.3 Viability of Higher-Salinity Smart Water Fluids

According to Seccombe *et al.* [52], software simulations using *PHREEQC* indicate that a 40 % pore volume slug of Smart Water brine is sufficient to benefit from a Smart Water effect throughout the reservoir, overcoming the change in salinity caused by diffusion between the injection brine and the existing connate water in the formation.

Seccombe *et al.* used a one-dimensional dispersion model—the concept of which has been criticized for being overly optimistic about incremental oil compared to two-dimensional 5-spot models, when evaluating slug sizes of over 20 % of the pore volume. A two-dimensional 5-spot model indicates that the effectiveness of a 40 % pore volume plug is around 67 % lower than a similarly sized slug in a one-dimensional setting. [53]

Seccombe *et al.* did report similar results in the core flooding experiments to back up their simulations. However—the spatial influence in a tiny rock specimen

is more or less negligible, as the core holder represents a no-flow boundary for the entire lateral area of the core. The core experiments are such that they can be treated as a one-dimensional system in this regard. Overall, this is a strong indication of a need for a larger slug size to overcome diffusion problematics. In light of this, the implementation of Smart Water flooding technology field-wide using the same assumptions as in the one-dimensional studies can quickly turn out to be detrimental for the project economy.

Understanding the true diffusion characteristics of the reservoir is of great importance when evaluating the possibility of using a brine with slightly higher salinity than a conventional low-salinity Smart Water. The diffusivity will dictate the salinity gradient and, because of an obvious inherent dependency, the slug size needed to ensure that the complete reservoir will benefit from the Smart Water flood.

This is where large-scale simulations can prove beneficial with regards to making the projects cost-effective. A set of salinity sensitivity diffusion simulations can be carried out, where the desired accuracy of the model will most likely necessitate the use of two-dimensional (or even three-dimensional) models. These sensitivity studies can perhaps suggest a series of plausible Smart Water compositions and corresponding slug sizes which can have the desired effect on the complete reservoir. The suggested brines can later be verified in laboratory core flooding experiments. Naturally, the complexity of the crude oil/rock/brine interaction means that these studies have to be repeated on a per-reservoir basis.

Successfully utilizing simulations in conjunction with experiments on cores can help increase the understanding of how to actually implement the Smart Water EOR method in developed fields and new fields alike, while retaining focus both on EOR effectiveness and economical optimization.

6 Conclusion

The findings of the thesis are summarized below;

1. The Yme-18 experiment suggests that 25.000 ppm brine is not able to produce Smart Water effects in the given system of crude oil and rock. The data indicates that the pH is buffered due to a relative increase in the replacement power of free Na^+ ions in solution versus H^+.

2. Depletion of anhydrite from the core material was not successful, and as such, getting reliable data to compare the difference between a core with an anhydrite presence and a clean core was not possible.

3. The Smart Water effects in Yme-19 and Yme-16 are within the margin of error associated with these types of experiments. However, very similar primary formation water flooding experiments can increase the integrity of the data. The 0.5 %OOIP discrepancy in increased recovery from low-salinity Smart Water can be explained by a combination of both elevated pH and calcium dissolution, which can lowers the wettability alteration potential in Yme-16 compared to Yme-19.

4. Precipitated calcium compounds can buffer the pH in the formation and dampen the release of organic components from the surface. With small concentrations of around just $1\,\mathrm{mmol\,L^{-1}}$ of sulfate in the effluent, the low-salinity Smart Water yield in two cores is only 2-2.5 %OOIP, much lower than expected from an ideal low-salinity Smart Water situation.

5. Indications of increased recovery from high-salinity reduction of capillary trapping observed in both Yme-19 and Yme-16 cores. The small incremental recovery is consistent with the proposed mechanisms and the apparent initial wetting conditions of the cores.

7 Future Work

The following bullet points describe my suggestions for future work which can be carried out by the EOR Team at the University of Stavanger, in relation to the experiments discussed in this thesis;

- As noted in the discussion of the Yme-18 results with regards to the low-salinity Smart Water effect—repeating this experiment and doing analyses on a full suite of effluent samples could help understand why the Smart Water effect was more pronounced during the 1.000 ppm flooding in Yme-18 compared to Yme-19 and Yme-16.

- If the excess calcium in the effluent observed in Yme-18 during the 25.000 ppm flood (Figure 20) comes from cationic exchange between Ca^{2+} and Na^{+} on the clay surface, this can be verified by extending the 25.000 ppm flood and analyze the effluent. If this holds true, the calcium values in the effluent samples should converge toward the sulfate values as the clay surface is depleted of calcium, as this will indicate that any calcium in the effluent originates from dissolution of anhydrite.

- Seeing as the oil used in the experiment had a good amount of basic organic material, but almost no acidic organic material, a different oil should be used in these "ideal" experiments. Perhaps mixing two oils which complement each other with regards to acid number and base number would constitute the best oil mixture for these experiments.

- If a critical pH threshold exists for a given core/brine/crude oil system, this can be verified by injecting successively less saline brines. Successive lowering of the salinity should incrementally raise the pH, until oil is produced at the threshold. This should be carried out in cores containing anhydrite, or with brines containing some small amount of calcium.

References

[1] Exxon Mobil Corporation. The outlook for energy: A view to 2040, 2014.

[2] Knut Bjørlykke. *Sedimentologi og Petroleumsgeologi*. Gyldendal Norsk Forlag, 2005.

[3] Joseph H. Spurk and Nuri Aksel. *Fluid Mechanics*. Springer-Verlag Berlin Heidelberg, 2. edition, 2008.

[4] John Grotzinger and Tom Jordan. *Understanding Earth*. W. H. Freeman and Company, 2010.

[5] Winfried Zimmerle. *Petroleum Sedimentology*. Kluwer Academic Publishers, 1995.

[6] Patrick James Dowey. *Prediction of clay minerals and grain-coatings in sandstone reservoirs utilising ancient examples and modern analogue studies*. PhD thesis, University of Liverpool, 2012.

[7] Alireza RezaeiDoust. *Low Salinity Water Flooding in Sandstone Reservoirs*. PhD thesis, University of Stavanger, 2011.

[8] P. J. Hamilton. A review of radiometric dating techniques for clay mineral cements in sandstones. *S.M. Richard H. Worden (Editor), Clay Mineral Cements in Sandstones*, 2009.

[9] IDF. *Clay Chemistry, Technical Manual for Drilling, Completion and Workover Fluids*. International Fluids Limited, 1982.

[10] F. Bergaya, B. K. G. Theng, and G. Lagaly. *Handbook of Clay Science*. Elsevier Science, 2006.

[11] Z. Zhou, W. D. Gunther, B. Kadatz, and S. Cameron. Effect of clay swelling on reservoir quality. *The Journal of Canadian Petroleum Technology*, 1996.

[12] Paul H. Nadeau, Steve N. Ehrenberg, and Øyvind Steen. Petroleum reservoir porosity versus depth: Influence of geological age. *The American Association of Petroleum Geologists*, 2009.

[13] Steve N. Ehrenberg, Paul H. Nadeau, and Øyvind Steen. A meagascale view of reservoir quality in producing sandstones from the offshore Gulf og Mexico. *E&P Note, The American Association of Petroleum Geologists*, 2008.

[14] T. Ahmed. Minimum Pressure Miscibility from EOS. *Petroleum Society's Canadian International Petroleum Conference*, 2000.

[15] Joseph R. Hearst, Philip H. Nelson, and Frederick L. Paillett. *Well Logging for Physical Properties*. John Wiley & Sons Ltd., 2. edition, 2000.

[16] Paul H. Nadeau and Steve N. Ehrenberg. Sandstone vs. carbonate petroleum reservoirs: A global perspective on porosity-depth and porosity-permeability relationships. *The American Association of Petroleum Geologists*, 2005.

[17] P. Zitha, R. Felder, D. Zornes, K. Brown, and K. Mohanty. Increasing hydrocarbon recovery factors. *SPE Technology Updates*, 2011.

[18] Tarek Ahmed and Paul D. McKinney. *Advanced Reservoir Engineering*. Gulf Professional Publishing, 2005.

[19] Don W. Green and G. Paul Willhite. *Enhanced Oil Recovery*. Society of Petroleum Engineers, 1998.

[20] European Central Bank. Risk-adjusted forecasts of oil prices, 2009.

[21] U.S. Energy Information Administration. Annual energy outlook, 2010.

[22] Enis Robbana, Todd Buikema, Chris Mair, Dale Williams, Dave Mercer, Kevin Webb, Aubrey Hewson, and Chris Reddick. Low Salinity Enhanced Oil Recovery - laboratory to day one field implementation - LoSal™ EOR into the Clair Ridge project. *SPE 161750, presented at the Abu Dhabi International Petroleum Exhibition & Conference held in Abu Dhabi, UAE, 11–14 November*, 2012.

[23] T. Austad and J. Milter. Spontaneous imbibition of water into low permeable chalk at different wettabilities using surfactants. *Society of Petroleum Engineers, presented at the International Symposium on Oilfield Chemistry, Houston, Texas, USA*, 1997.

[24] T. Ahmed. *Reservoir Engineering Handbook*. Gulf Publishing, 2000.

[25] William G. Anderson. Wettability literature survey–part 2: Wettability measurement. *Journal of Petroleum Technology*, 1986.

[26] Anatoly B. Zolothukin and Jann-Rune Ursin. *Introduction to Petroleum Engineering*. Høyskoleforlaget, 2000.

[27] T. F. Moore and R. L. Slobod. The effect of viscosity and capillarity on the displacement of oil by water. *Prod. Monthly*, August 1956.

[28] A. Abrams. The influence of fluid viscosity, interfacial tension, and flow velocity on residual oil saturation left by waterflood. *Society of Petroleum Engineers Journal*, 1974.

[29] F. F. Jr. Craig. The reservoir engineering aspects of waterflooding. *Society of Petroleum Engineers of AIME*, 1971.

[30] Earl Amott. Observations relating to the wettability of porous rock. *Petroleum Transactions, AIME*, Vol. 216, 1959.

[31] R. D. Thomas E. C. Donaldson and P. B. Lorenz. Wettability determination and its effect on recovery efficiency. *Society of Petroleum Engineers Journal*, 1969.

[32] L. E. Treiber, Duane L. Archer, and W. W. Owens. A laboratory evaluation of the wettability of fifty oil-producing reservoirs. *Society of Petroleum Engineers Journal*, 1972.

[33] Norman R. Morrow. Capillary pressure correlations for uniformly wetted porous media. *The Journal of Canadian Petroleum Technology*, 1976.

[34] Nanji J. Hadia, Adeel Ashraf, Medad T. Tweheyo, and Ole Torsæter. Laboratory investigation on effects of initial wettabilities on performance of low salinity waterflooding. *Journal of Petroleum Science and Engineering*, 2013.

[35] Skule Strand, Tina Puntervold, and Tor Austad. Water based EOR from clastic oil reservoirs by wettability alteration: A chemical evaluation. *Currently Unpublished Article*, 2014.

[36] Sitthisak Prasanphan and Apinon Nuntiya. Electrokinetic properties of kaolins, sodium feldspar and quartz. *Chiang Mai J. Sci.*, 2006.

[37] Lene Madsen and Ida Lind. Adsorption of carboxylic acids on reservoir minerals from organic and aqueous phase. *SPE Reservoir Evaluation & Engineering*, 1998.

[38] Guo-qing Tang and Norman R. Morrow. Salinity, temperature, oil composition, and oil recovery by waterflooding. *SPE Reservoir Engineering*, Vol. 12, 1997.

[39] Norman R. Morrow, Guo-qing Tang, Marc Valat, and Xina Xie. Prospects of improved oil recovery related to wettability and brine composition. *Journal of Petroleum Science and Engineering*, Vol. 20, 1998.

[40] Guo-qing Tang and Norman R. Morrow. Oil recovery by waterflooding and imbibition—invading brine cation valency and salinity. *International Symposium of the Society of Core Analysts, 1-4 August, Golden, Colorado, USA*, 1999.

[41] Jim Seccombe, Arnaud Lager, Gary Jerauld, Bharat Jhaveri, Todd Buikema, Sierra Bassler, John Denis, Kevin Webb, Andrew Cockin, and Esther Fueg. Demonstration of low-salinity EOR at interwell scale, Endicott Field, Alaska. *SPE Improved Oil Recovery Symposium, 24-28 April, Tulsa, Oklahoma, USA*, 2010.

[42] Guo-qing Tang and Norman R. Morrow. Influence of brine composition and fines migration on crude oil/brine/rock interactions and oil recovery. *Journal of Petroleum Science Engineering*, Vol. 24, 1999.

[43] P. L. McGuire, J. R. Chatham, F. K. Paskvan, D. M. Sommer, and F. H. Carini. Low salinity oil recovery: An exciting new EOR opportunity for Alaska's North Slope. *SPE 93903, presented at the 2005 SPE Western Regional Meeting, Irvine, California, USA*, 2005.

[44] A. Lager, K. J. Webb, and C. J. J. Black. Impact of brine chemistry on oil recovery. *Paper A24, presented at the 14th European Symposium on Improved Oil Recovery, Cairo, Egypt*, 2007.

[45] A. Skauge. Microscopic diversion—A new EOR technique. *Presented at the 29th IEA Workshop & Symposium, Beijing*, 2008.

[46] D. J. Ligthelm, J. Gronsveld, J. P. Hofman, N. J. Brussee, F. Marcelis, and H. A. van der Linde. Novel waterflooding strategy by manipulation of injection brine composition. *SPE 119835, presented at the 2009 SPE EUROPEC/EAGE Annual Conference and Exhibition, Amsterdam, The Netherlands*, 2009.

[47] Tor Austad, Alireza RezaeiDoust, and Tina Puntervold. Chemical mechanism of low salinity water flooding in sandstone reservoirs. *SPE 129767, presented at the Improved Oil Recovery Symposium, Tulsa, Oklahoma, USA*, 2010.

[48] Hakan Aksulu, Dagny Håmsø, Skule Strand, Tina Puntervold, and Tor Austad. Evaluation of low-salinity enhanced oil recovery effects in sandstone: Effects of the temperature and pH gradient. *Energy & Fuels*, Vol. 26, 2012.

[49] Alireza RezaeiDoust, Tina Puntervold, and Tor Austad. A discussion of the low salinity EOR potential for a North Sea sandstone field. *SPE 134459, presented at the SPE Annual Technical Conference and Exhibition held in Florence, Italy*, 2012.

[50] M. M. Sharma and P. R. Filco. Effect of brine salinity and crude-oil properties on oil recovery and residual saturations. *SPE 65402, SPE Journal*, Vol. 5, 2000.

[51] Yongsheng Zhang and Norman R. Morrow. Comparison of secondary and tertiary recovery with change in injection brine composition for crude oil/sandstone combinations. *SPE 99757, presented at SPE/DOE Symposium on Improved Oil Recovery, 22-26 April, Tulsa, Oklahoma, USA*, 2006.

[52] James C. Seccombe, Arnaud Lager, Kevin Webb, Gary Jerauld, and Esther Fueg. Improving waterflood recovery: LoSal™ EOR Field Evaluation. *SPE 113480, presented at SPE/DOE Symposium on Improved Oil Recovery, 19-23 April, Tulsa, Oklahoma, USA*, 2008.

[53] G.R. Jerauld, C.Y. Lin, K.J. Webb, and J.C. Seccombe. Modeling low-salinity waterflooding. *SPE 102239, presented at the 2006 SPE Annual Technical Conference and Exhibition, 24–27 September, San Antonio, Texas, USA*, 2006.

[54] N. Springer, U. Korsbech, and H. K. Aage. Resistivity index measurement without the porous plate: A desaturation technique based on evaporation produces uniform water saturation profiles and more reliable results for tight North Sea chalk. *International Symposium of the Society of Core Analysts, Pau, France*, 2003.